

Impact of recent measurement of $(g - 2)_\mu$, LHC search for supersymmetry, and LZ experiment on Minimal Supersymmetric Standard Model

Yangle He^a, Xinglong Jia^a, Lei Meng^{a,*}, Yuanfang Yue^a, and Di Zhang^a

^a *Department of Physics, Henan Normal University, Xinxiang 453007, China*

E-mail: heyangle@htu.edu.cn, JiaXinglong1996@outlook.com,
mel18@foxmail.com, yueyuanfang@htu.edu.cn, dz481655@gmail.com

ABSTRACT: Motivated by the recent measurement of muon anomalous magnetic moment at Fermilab, the rapid progress of the LHC search for supersymmetry, and the significantly improved sensitivities of dark matter direct detection experiments, we studied their impacts on the Minimal Supersymmetric Standard Model (MSSM). We conclude that higgsino mass should be larger than about 500 GeV for $M_1 < 0$ and 630 GeV for $M_1 > 100$ GeV, where M_1 denotes the bino mass. These improved bounds imply a tuning of $\mathcal{O}(1\%)$ to predict the Z -boson mass and simultaneously worsen the naturalness of the Z - and h -mediated resonant annihilations to achieve the measured dark matter density. We also concluded that the LHC restrictions have set lower bounds on the sparticle mass spectra: $m_{\tilde{\chi}_1^0} \gtrsim 210$ GeV, $m_{\tilde{\chi}_2^0}, m_{\tilde{\chi}_1^\pm} \gtrsim 235$ GeV, $m_{\tilde{\chi}_3^0} \gtrsim 515$ GeV, $m_{\tilde{\chi}_4^0} \gtrsim 525$ GeV, $m_{\tilde{\chi}_2^\pm} \gtrsim 530$ GeV, $m_{\tilde{\nu}_\mu} \gtrsim 235$ GeV, $m_{\tilde{\mu}_1} \gtrsim 215$ GeV, and $m_{\tilde{\mu}_2} \gtrsim 250$ GeV, where $\tilde{\chi}_2^0$ and $\tilde{\chi}_1^\pm$ are wino-dominated when they are lighter than about 500 GeV. These bounds are far beyond the reach of the LEP experiments in searching for supersymmetry and have not been acquired before. In addition, we illuminate how some parameter spaces of the MSSM have been tested at the LHC and provide five scenarios in which the theory coincides with the LHC restrictions. Once the muon $g-2$ anomaly is confirmed to originate from supersymmetry, this research may serve as a guide to explore the characteristics of the MSSM in future experiments.

Keywords: Supersymmetry, MSSM, muon anomalous magnetic moment, the LHC search for SUSY, LZ experiment.

*Corresponding author.

Contents

1	Introduction	2
2	Theoretical preliminaries of Minimal Supersymmetric Standard Model (MSSM)	3
2.1	Dark matter (DM) physics in MSSM	3
2.2	Muon $g-2$	5
2.3	LHC search for SUSY	6
3	Combined experimental impacts on MSSM	9
3.1	Research strategy	9
3.2	Key features of the results	11
3.3	More details of LHC restrictions	18
3.4	Related issues	23
4	Summary	24
5	Acknowledgement	25

1 Introduction

As the cornerstone of particle physics, the Standard Model (SM) has encapsulated our best understanding of fundamental particles and forces. Although it is well tested by many experimental results, there are still unsolved puzzles, such as the quadratic divergence in the Higgs squared mass and the absence of dark matter (DM) candidates. Historically, these puzzles were viewed as robust evidence of new physics beyond the SM, and looking for mechanisms to circumvent them was the model-building guideline. Supersymmetry (SUSY) is the most promising among the new physics theories due to its elegant structure and remarkable advantages in solving these puzzles [1–4].

To date, rich information about SUSY has been accumulated due to the rapid progress of particle physics experiments in recent years. The Run-II data of the Large Hadron Collider (LHC) enabled scientists to explore the properties of winos, higgsinos, and scalar leptons (sleptons), which are the SUSY partners of W , Higgs, and lepton fields, respectively. It was found that wino masses up to about 1060 GeV for $m_{\tilde{\chi}_1^0} \lesssim 400$ GeV and higgsino masses up to 900 GeV for $m_{\tilde{\chi}_1^0} \lesssim 240$ GeV have been excluded in the simplified model of SUSY [5], where $\tilde{\chi}_1^0$ denotes the lightest neutralino, acting as the lightest supersymmetric particle (LSP) and thus a DM candidate under the assumption of R -parity conservation [4], and $m_{\tilde{\chi}_1^0}$ is its mass. The data also excluded sleptons lighter than approximately 700 GeV when the LSP was massless based on statistical methods [5, 6]. Furthermore, the LUX-ZEPLIN (LZ) experiment just released its first results about the direct search for DM, where the sensitivities to spin-independent (SI) and spin-dependent (SD) cross sections of DM-nucleon scattering have reached about 6.0×10^{-48} cm² and 1.0×10^{-42} cm², respectively, for the DM mass around 30 GeV [7]. These unprecedented precision values strongly limit the DM coupling to the SM particles, which are determined by SUSY parameters. In addition, the combined measurement of the muon anomalous magnetic moment, $a_\mu \equiv (g - 2)_\mu/2$, by the E821 experiment at the Brookhaven National Laboratory (BNL) [8] and the E989 experiment at Fermilab [9] indicates a 4.2σ discrepancy from the SM’s prediction [10–30]. Although this difference may have been induced by the uncertainties in calculating the hadronic contribution to the moment, as revealed by the recent lattice simulation of the BMW collaboration [31], it was widely speculated to arise from new physics (see, e.g., Ref. [32] and the references therein). Along this direction, it is remarkable that once the difference is confirmed to originate from SUSY effects, salient features of the theory, e.g., the mass spectra of the electroweakinos and sleptons, can be inferred [33–89].

Given that SUSY predictions on these experimental results rely on different theoretical inputs, it is essential to collectively study their impacts on the Minimal Supersymmetric Standard Model (MSSM), which is the most economical realization of SUSY in particle physics [2, 90, 91]. For this purpose, we organize this study as

follows. In Sec. 2, we briefly introduce the basics of the MSSM, including its DM physics, the SUSY contribution to a_μ , the signals of SUSY particles (sparticles) at the LHC, and the strategy to search for them. In Sec. 3, we perform a sophisticated scan over the broad parameter space of the MSSM and clarify how the MSSM remains consistent with the experimental results. Finally, we draw conclusions in Sec. 4.

2 Theoretical preliminaries of Minimal Supersymmetric Standard Model (MSSM)

The following superpotential of the MSSM was given in Ref. [2, 90]:

$$W = -Y_d \hat{q} \cdot \hat{H}_d \hat{d} - Y_e \hat{l} \cdot \hat{H}_d \hat{e} + Y_u \hat{q} \cdot \hat{H}_u \hat{u} + \mu \hat{H}_u \cdot \hat{H}_d, \quad (2.1)$$

where the superfields \hat{q} and \hat{l} are left-handed SU(2) doublets for quarks and leptons, respectively, and \hat{u} , \hat{d} , and \hat{e} are right-handed singlets for fermions. The scalar components of the Higgs doublet superfields, \hat{H}_u and \hat{H}_d , are given by $H_u = (H_u^+, H_u^0)$ and $H_d = (H_d^0, H_d^-)$, respectively, and their product is defined by $H_u \cdot H_d = (H_u^+ H_d^- - H_u^0 H_d^0)$. The first three terms in the superpotential represent the Yukawa couplings of the quark and lepton fields, and the last term is responsible for the higgsino mass.

The MSSM predicts two CP-even Higgs bosons, h and H , one CP-odd Higgs boson A , and a pair of charged Higgs boson $H^\pm = \cos \beta H_u^\pm + \sin \beta H_d^\pm$ in the Higgs sector [90, 91]. Among these states, h denotes the SM-like scalar discovered at the LHC with $m_h \simeq 125$ GeV, and the neutral states H and A are approximately degenerate with H^\pm in mass. The LHC search for non-SM-like Higgs bosons has obtained model-independent upper limits on the production rates of H , A , and H^\pm (see, e.g., Ref. [92, 93]), indicating that they should be massive. The electroweakino sector of the MSSM consists of four neutralinos and two pairs of charginos [90], denoted by $\tilde{\chi}_i^0$ with $i = 1, 2, 3, 4$ and $\tilde{\chi}_j^\pm$ with $j = 1, 2$, respectively, in this work. The neutralinos are superpositions of bino (\tilde{B}), wino (\tilde{W}^0), and two higgsino fields (\tilde{H}_d^0 and \tilde{H}_u^0), and they are majorana fermions. By contrast, the left-handed and right-handed components of the chargino $\tilde{\chi}_j^\pm$ come from the mixing of \tilde{W}^+ with \tilde{H}_u^+ and \tilde{W}^- with \tilde{H}_d^- , respectively. Thus, $\tilde{\chi}_j^\pm$ are Dirac fermions. By convention, the neutralinos as mass eigenstates are labeled in ascending mass order, and so are the charginos. In addition, each slepton mass eigenstate in the MSSM is associated with a definite flavor quantum number if there is no flavor mixing in the slepton sector [94, 95]. The ℓ -flavored sleptons $\tilde{\ell}_i$ ($i=1,2$) are mixtures of chiral scalar fields $\tilde{\ell}_L$ and $\tilde{\ell}_R$. Given that the mixing is usually small, we also denote $\tilde{\ell}_i$ by its dominant component sometimes to facilitate our discussion.

2.1 Dark matter (DM) physics in MSSM

On the premise of explaining both the measured DM density and the muon $g-2$ anomaly, the DM candidate in the MSSM must be the bino-dominated lightest neu-

tralino [96]¹. It achieves the measured density through the co-annihilation with wino-dominated electroweakinos or sleptons, or through Z - or h -mediated resonant annihilation [99]. In the co-annihilation case, the reactions $S_i S_j \rightarrow XX'$, where $S_i S_j$ may be LSP-LSP, LSP-NLSP (next lightest supersymmetric particle), and NLSP-NLSP annihilation states and XX' denotes SM particles, contribute to the density [100, 101]. The effective annihilation rate at a temperature T is then given by Eq. (3.2) in Ref. [101]. This formula indicates that the annihilation partner only has a significant effect when the departure of its mass from the DM mass is less than about 10%. The resonant annihilation is distinct in that the density is very sensitive to the splitting between $2|m_{\tilde{\chi}_1^0}|$ and the mediator's mass [99]. The weaker the DM coupled to the mediator, the smaller the splitting must be to obtain the measured density. Evidently, this situation requires the fine-tuning of the theoretical parameters.

The cross sections of the DM-nucleon scattering are approximated by [102, 103]

$$\sigma_{\tilde{\chi}_1^0-N}^{\text{SI}} \simeq 5 \times 10^{-45} \text{cm}^2 \left(\frac{C_{\tilde{\chi}_1^0 \tilde{\chi}_1^0 h}}{0.1} \right)^2 \left(\frac{m_h}{125 \text{GeV}} \right)^2, \quad (2.2)$$

$$\sigma_{\tilde{\chi}_1^0-N}^{\text{SD}} \simeq C_N \times \left(\frac{C_{\tilde{\chi}_1^0 \tilde{\chi}_1^0 Z}}{0.1} \right)^2, \quad (2.3)$$

where $C_p \simeq 1.8 \times 10^{-40} \text{cm}^2$ for protons, $C_n \simeq 1.4 \times 10^{-40} \text{cm}^2$ for neutrons, and $C_{\tilde{\chi}_1^0 \tilde{\chi}_1^0 h}$ and $C_{\tilde{\chi}_1^0 \tilde{\chi}_1^0 Z}$ represent DM couplings to the SM-like Higgs boson and Z -boson, respectively. These couplings take the following form [104–106]:

$$\begin{aligned} C_{\tilde{\chi}_1^0 \tilde{\chi}_1^0 h} &\simeq e \tan \theta_W \frac{m_Z}{\mu(1 - m_{\tilde{\chi}_1^0}^2/\mu^2)} \left(\cos(\beta + \alpha) + \sin(\beta - \alpha) \frac{m_{\tilde{\chi}_1^0}}{\mu} \right) \\ &\simeq e \tan \theta_W \frac{m_Z}{\mu(1 - m_{\tilde{\chi}_1^0}^2/\mu^2)} \left(\sin 2\beta + \frac{m_{\tilde{\chi}_1^0}}{\mu} \right), \end{aligned} \quad (2.4)$$

$$C_{\tilde{\chi}_1^0 \tilde{\chi}_1^0 Z} \simeq \frac{e \tan \theta_W \cos 2\beta}{2} \frac{m_Z^2}{\mu^2 - m_{\tilde{\chi}_1^0}^2}, \quad (2.5)$$

where θ_W is the weak mixing angle, the DM mass $m_{\tilde{\chi}_1^0}$ relates to the bino mass M_1 by $m_{\tilde{\chi}_1^0} \simeq M_1$, $\tan \beta = v_u/v_d$ is the ratio of Higgs vacuum expectation values, and α is the mixing angle of the CP-even Higgs states satisfying $\alpha \simeq \beta - \pi/2$ in the large m_A limit [91]. The formulae for the SI scattering indicate that if M_1 and μ are of the same sign, μ must be sufficiently large to be consistent with the results of the PandaX-4T experiment [107]. These formulas also show that if M_1 and μ are of

¹In the case that the lightest left-handed sneutrino acts as a DM candidate, its interaction with Z -boson predicts a much smaller density than its measured value, i.e., $\Omega h^2 \ll 0.12$, and meanwhile an unacceptably large DM-nucleon scattering rate [97]. For the wino- or higgsino-dominated DM case, the density is on the order of 10^{-3} by our calculation. These cases were surveyed in the MSSM to explain the muon $g-2$ anomaly in Ref. [98].

opposite signs, which can result in the blind spots of the scattering [108–111], $|\mu| \sim 100$ GeV seems to be experimentally allowed. However, such a possibility has been limited by the experimental search for spin-dependent (SD) DM-nucleon scattering because, regardless of the relative sign between M_1 and μ , a small $|\mu|$ can enhance the scattering cross section. In summary, the DM direct detection experiments alone can set a lower bound on the magnitude of μ . With the improvement of the experimental sensitivity, the bound will become tightened.

2.2 Muon g-2

The SUSY source of the muon g-2, a_μ^{SUSY} , mainly includes loops mediated by a smuon and a neutralino and those containing a muon-flavor sneutrino and a chargino [33–36]. The full one-loop contributions to a_μ^{SUSY} in the MSSM are not presented here for brevity. Instead, we provide the expression of a_μ^{SUSY} in the mass insertion approximation to reveal its key features [35]. Specifically, at the lowest order of the approximation, the contributions to a_μ^{SUSY} are divided into four types: "WHL," "BHL," "BHR," and "BLR," where W , B , H , L , and R represent wino, bino, higgsino, and left-handed and right-handed smuon fields, respectively. They arise from the Feynman diagrams involving $\tilde{W} - \tilde{H}_d$, $\tilde{B} - \tilde{H}_d^0$, $\tilde{B} - \tilde{H}_d^0$, and $\tilde{\mu}_L - \tilde{\mu}_R$ transitions, respectively, and take the following forms [35, 37, 38]:

$$a_{\mu, \text{WHL}}^{\text{SUSY}} = \frac{\alpha_2 m_\mu^2 M_2 \mu_{\text{tot}} \tan \beta}{8\pi m_{\tilde{\nu}_\mu}^4} \left\{ 2f_C \left(\frac{M_2^2}{m_{\tilde{\nu}_\mu}^2}, \frac{\mu_{\text{tot}}^2}{m_{\tilde{\nu}_\mu}^2} \right) - \frac{m_{\tilde{\nu}_\mu}^4}{\tilde{m}_{\tilde{\mu}_L}^4} f_N \left(\frac{M_2^2}{\tilde{m}_{\tilde{\mu}_L}^2}, \frac{\mu_{\text{tot}}^2}{\tilde{m}_{\tilde{\mu}_L}^2} \right) \right\}, \quad (2.6)$$

$$a_{\mu, \text{BHL}}^{\text{SUSY}} = \frac{\alpha_Y m_\mu^2 M_1 \mu_{\text{tot}} \tan \beta}{8\pi \tilde{m}_{\tilde{\mu}_L}^4} f_N \left(\frac{M_1^2}{\tilde{m}_{\tilde{\mu}_L}^2}, \frac{\mu_{\text{tot}}^2}{\tilde{m}_{\tilde{\mu}_L}^2} \right), \quad (2.7)$$

$$a_{\mu, \text{BHR}}^{\text{SUSY}} = -\frac{\alpha_Y m_\mu^2 M_1 \mu_{\text{tot}} \tan \beta}{4\pi \tilde{m}_{\tilde{\mu}_R}^4} f_N \left(\frac{M_1^2}{\tilde{m}_{\tilde{\mu}_R}^2}, \frac{\mu_{\text{tot}}^2}{\tilde{m}_{\tilde{\mu}_R}^2} \right), \quad (2.8)$$

$$a_{\mu, \text{BLR}}^{\text{SUSY}} = \frac{\alpha_Y m_\mu^2 M_1 \mu_{\text{tot}} \tan \beta}{4\pi M_1^4} f_N \left(\frac{\tilde{m}_{\tilde{\mu}_L}^2}{M_1^2}, \frac{\tilde{m}_{\tilde{\mu}_R}^2}{M_1^2} \right), \quad (2.9)$$

where $\tilde{m}_{\tilde{\mu}_L}$ and $\tilde{m}_{\tilde{\mu}_R}$ are soft-breaking masses for left-handed and right-handed smuon fields, respectively, at the slepton mass scale. They are approximately equal to slepton masses. The loop functions are given by

$$f_C(x, y) = \frac{5 - 3(x + y) + xy}{(x - 1)^2(y - 1)^2} - \frac{2 \ln x}{(x - y)(x - 1)^3} + \frac{2 \ln y}{(x - y)(y - 1)^3}, \quad (2.10)$$

$$f_N(x, y) = \frac{-3 + x + y + xy}{(x - 1)^2(y - 1)^2} + \frac{2x \ln x}{(x - y)(x - 1)^3} - \frac{2y \ln y}{(x - y)(y - 1)^3}, \quad (2.11)$$

and they satisfy $f_C(1, 1) = 1/2$ and $f_N(1, 1) = 1/6$.

The following points about a_μ^{SUSY} should be noted:

- If all the dimensional SUSY parameters involved in a_μ^{SUSY} take a common value M_{SUSY} , a_μ^{SUSY} is proportional to $m_\mu^2 \tan \beta / M_{\text{SUSY}}^2$, indicating that the muon g-2 anomaly prefers a large $\tan \beta$ and a moderately low SUSY scale.

- The "WHL" contribution is usually much larger than the other contributions if $\tilde{\mu}_L$ is not significantly heavier than $\tilde{\mu}_R$ [72].
- The difference between the a_μ^{SUSY} values calculated by the mass insertion approximation and the full expression was less than 3%. We verified this conclusion for the green samples in Fig. 1 of this work.
- The two-loop (2L) contributions to a_μ , including 2L corrections to SM one-loop diagrams and those to SUSY one-loop diagrams [39], were about -5% of the one-loop prediction [89]. These were neglected in this study.

2.3 LHC search for SUSY

Since some of the electroweakinos and sleptons involved in a_μ^{SUSY} must be moderately light to account for the anomaly [84], they are copiously produced at the LHC and thus are subjected to strong constraints from the SUSY searches at the LHC with $\sqrt{s} = 13$ TeV. These searches usually concentrate on theories with R -parity conservation [128, 129], where the LSP is undetected, leading to missing energy in the final states. We implement these restrictions by scrutinizing the experimental analyses in Tables 1 and 2. We find that the following reports are particularly critical:

- CMS-SUS-20-001 [6]: Search for SUSY signal containing two oppositely charged same-flavor leptons and missing transverse momentum. This analysis studied not only strong sparticle productions but also electroweakino productions. The lepton originates from an on-shell or off-shell Z boson in the decay chain or from the decay of the produced sleptons. For the electroweakino pair production, the wino-dominated chargino and neutralino were explored up to masses of 750 GeV and 800 GeV, respectively. For the slepton pair production, the first two-generation sleptons were explored up to a mass of 700 GeV.
- CMS-SUS-16-039 and CMS-SUS-17-004 [113, 114]: Search for electroweakino productions with two, three, or four leptons and missing transverse momentum (E_T^{miss}) in the final states. One remarkable strategy of this analysis was that it included all the possible final states and defined several categories by the number of leptons in the event, their flavors, and their charges to enhance the discovery potential. In the context of simplified models, the observed limit on wino-dominated $m_{\tilde{\chi}_1^\pm}$ in the chargino-neutralino production was about 650 GeV for the WZ topology, 480 GeV for the WH topology, and 535 GeV for the mixed topology.
- ATLAS-2106-01676 [112]: Searched for wino- or higgsino-dominated chargino-neutralino pair productions. This analysis investigated on-shell WZ , off-shell WZ , and Wh categories in the decay chain and focused on the final state containing exactly three leptons, possible ISR jets, and E_T^{miss} . For the wino scenario

Table 1. Experimental analyses of the electroweakino production processes considered in this study, which are categorized by the topologies of the supersymmetry (SUSY) signals.

Scenario	Final State	Name
$\tilde{\chi}_2^0 \tilde{\chi}_1^\pm \rightarrow W Z \tilde{\chi}_1^0 \tilde{\chi}_1^0$	$n\ell(n \geq 2) + nj(n \geq 0) + E_T^{\text{miss}}$	CMS-SUS-20-001(137fb ⁻¹) [6]
		ATLAS-2106-01676(139fb ⁻¹) [112]
		CMS-SUS-17-004(35.9fb ⁻¹) [113]
		CMS-SUS-16-039(35.9fb ⁻¹) [114]
		ATLAS-1803-02762(36.1fb ⁻¹) [115]
		ATLAS-1806-02293(36.1fb ⁻¹) [116]
$\tilde{\chi}_2^0 \tilde{\chi}_1^\pm \rightarrow \ell \tilde{\nu} \ell \tilde{\ell}$	$n\ell(n = 3) + E_T^{\text{miss}}$	CMS-SUS-16-039(35.9fb ⁻¹) [114]
		ATLAS-1803-02762(36.1fb ⁻¹) [115]
$\tilde{\chi}_2^0 \tilde{\chi}_1^\pm \rightarrow \tilde{\tau} \nu \ell \tilde{\ell}$	$2\ell + 1\tau + E_T^{\text{miss}}$	CMS-SUS-16-039(35.9fb ⁻¹) [114]
$\tilde{\chi}_2^0 \tilde{\chi}_1^\pm \rightarrow \tilde{\tau} \nu \tilde{\tau} \tau$	$3\tau + E_T^{\text{miss}}$	CMS-SUS-16-039(35.9fb ⁻¹) [114]
$\tilde{\chi}_2^0 \tilde{\chi}_1^\pm \rightarrow W h \tilde{\chi}_1^0 \tilde{\chi}_1^0$	$n\ell(n \geq 1) + nb(n \geq 0) + nj(n \geq 0) + E_T^{\text{miss}}$	ATLAS-1909-09226(139fb ⁻¹) [117]
		CMS-SUS-17-004(35.9fb ⁻¹) [113]
		CMS-SUS-16-039(35.9fb ⁻¹) [114]
		ATLAS-1812-09432(36.1fb ⁻¹) [118]
		CMS-SUS-16-034(35.9fb ⁻¹) [119]
		CMS-SUS-16-045(35.9fb ⁻¹) [120]
$\tilde{\chi}_1^\mp \tilde{\chi}_1^\pm \rightarrow W W \tilde{\chi}_1^0 \tilde{\chi}_1^0$	$2\ell + E_T^{\text{miss}}$	ATLAS-1908-08215(139fb ⁻¹) [5]
		CMS-SUS-17-010(35.9fb ⁻¹) [121]
$\tilde{\chi}_1^\mp \tilde{\chi}_1^\pm \rightarrow 2\tilde{\ell} \nu(\tilde{\nu} \ell)$	$2\ell + E_T^{\text{miss}}$	ATLAS-1908-08215(139fb ⁻¹) [5]
		CMS-SUS-17-010(35.9fb ⁻¹) [121]
$\tilde{\chi}_2^0 \tilde{\chi}_1^\mp \rightarrow h/ZW \tilde{\chi}_1^0 \tilde{\chi}_1^0, \tilde{\chi}_1^0 \rightarrow \gamma/Z\tilde{G}$ $\tilde{\chi}_1^\pm \tilde{\chi}_1^\mp \rightarrow W W \tilde{\chi}_1^0 \tilde{\chi}_1^0, \tilde{\chi}_1^0 \rightarrow \gamma/Z\tilde{G}$	$2\gamma + n\ell(n \geq 0) + nb(n \geq 0) + nj(n \geq 0) + E_T^{\text{miss}}$	ATLAS-1802-03158(36.1fb ⁻¹) [122]
$\tilde{\chi}_2^0 \tilde{\chi}_1^\pm \rightarrow ZW \tilde{\chi}_1^0 \tilde{\chi}_1^0, \tilde{\chi}_1^0 \rightarrow h/Z\tilde{G}$ $\tilde{\chi}_1^\pm \tilde{\chi}_1^\mp \rightarrow W W \tilde{\chi}_1^0 \tilde{\chi}_1^0, \tilde{\chi}_1^0 \rightarrow h/Z\tilde{G}$ $\tilde{\chi}_2^0 \tilde{\chi}_1^0 \rightarrow Z\tilde{\chi}_1^0 \tilde{\chi}_1^0, \tilde{\chi}_1^0 \rightarrow h/Z\tilde{G}$ $\tilde{\chi}_1^\mp \tilde{\chi}_1^0 \rightarrow W \tilde{\chi}_1^0 \tilde{\chi}_1^0, \tilde{\chi}_1^0 \rightarrow h/Z\tilde{G}$	$n\ell(n \geq 4) + E_T^{\text{miss}}$	ATLAS-2103-11684(139fb ⁻¹) [123]
$\tilde{\chi}_i^{0,\pm} \tilde{\chi}_j^{0,\mp} \rightarrow \tilde{\chi}_1^0 \tilde{\chi}_1^0 + \chi_{\text{soft}} \rightarrow ZZ/H\tilde{G}\tilde{G}$	$n\ell(n \geq 2) + nb(n \geq 0) + nj(n \geq 0) + E_T^{\text{miss}}$	CMS-SUS-16-039(35.9fb ⁻¹) [114]
		CMS-SUS-17-004(35.9fb ⁻¹) [113]
		CMS-SUS-20-001(137fb ⁻¹) [6]
$\tilde{\chi}_i^{0,\pm} \tilde{\chi}_j^{0,\mp} \rightarrow \tilde{\chi}_1^0 \tilde{\chi}_1^0 + \chi_{\text{soft}} \rightarrow HH\tilde{G}\tilde{G}$	$n\ell(n \geq 2) + nb(n \geq 0) + nj(n \geq 0) + E_T^{\text{miss}}$	CMS-SUS-16-039(35.9fb ⁻¹) [114]
		CMS-SUS-17-004(35.9fb ⁻¹) [113]
$\tilde{\chi}_2^0 \tilde{\chi}_1^\pm \rightarrow W^* Z^* \tilde{\chi}_1^0 \tilde{\chi}_1^0$	$3\ell + E_T^{\text{miss}}$	ATLAS-2106-01676(139fb ⁻¹) [112]
$\tilde{\chi}_2^0 \tilde{\chi}_1^\pm \rightarrow Z^* W^* \tilde{\chi}_1^0 \tilde{\chi}_1^0$	$2\ell + nj(n \geq 0) + E_T^{\text{miss}}$	ATLAS-1911-12606(139fb ⁻¹) [124]
		ATLAS-1712-08119(36.1fb ⁻¹) [125]
		CMS-SUS-16-048(35.9fb ⁻¹) [126]
$\tilde{\chi}_2^0 \tilde{\chi}_1^\pm + \tilde{\chi}_1^\pm \tilde{\chi}_1^\mp + \tilde{\chi}_1^\pm \tilde{\chi}_1^0$	$2\ell + nj(n \geq 0) + E_T^{\text{miss}}$	ATLAS-1911-12606(139fb ⁻¹) [124]
		ATLAS-1712-08119(36.1fb ⁻¹) [125]
		CMS-SUS-16-048(35.9fb ⁻¹) [126]

in the simplified model, the exclusion bound of $m_{\tilde{\chi}_2^0}$ was about 640 GeV for a massless $\tilde{\chi}_1^0$, and it was weakened as the mass difference between $\tilde{\chi}_2^0$ and $\tilde{\chi}_1^0$ diminished. Specifically, $\tilde{\chi}_2^0$ should be heavier than about 500 GeV for

Table 2. Same as Table 1, but for the slepton production processes.

Scenario	Final State	Name
$\tilde{\ell}\tilde{\ell} \rightarrow \ell\ell\tilde{\chi}_1^0\tilde{\chi}_1^0$	$2\ell + E_T^{\text{miss}}$	ATLAS-1911-12606 (139 fb ⁻¹) [124]
		ATLAS-1712-08119 (36.1 fb ⁻¹) [125]
		ATLAS-1908-08215 (139 fb ⁻¹) [5]
		CMS-SUS-20-001 (137 fb ⁻¹) [6]
		ATLAS-1803-02762 (36.1 fb ⁻¹) [115]
		CMS-SUS-17-009 (35.9 fb ⁻¹) [127]

Table 3. Parameter space explored in this study. Other dimensional parameters not crucial to this study were fixed at 3 TeV, including the SUSY parameters for the first- and third-generation sleptons, three generation squarks (except for the soft trilinear coefficients A_t and A_b , which are assumed to be equal and change freely), and gluinos. All the parameters were defined at the renormalization scale $Q = 1$ TeV.

Parameter	Prior	Range	Parameter	Prior	Range
$\tan\beta$	Flat	$1 \sim 60$	A_t/TeV	Flat	$-5.0 \sim 5.0$
μ/TeV	Log	$0.1 \sim 1.0$	m_A/TeV	Log	$0.5 \sim 10$
M_1/TeV	Flat	$-1.5 \sim 1.5$	M_2/TeV	Log	$0.1 \sim 1.5$
$\tilde{m}_{\tilde{\mu}_L}/\text{TeV}$	Log	$0.1 \sim 1.0$	$\tilde{m}_{\tilde{\mu}_R}/\text{TeV}$	Log	$0.1 \sim 1.0$

$m_{\tilde{\chi}_1^0} = 300$ GeV (the on-shell W/Z case), 300 GeV for a positive $m_{\tilde{\chi}_1^0}$ and 35 GeV $\lesssim m_{\tilde{\chi}_2^0} - m_{\tilde{\chi}_1^0} \lesssim 90$ GeV (the off-shell W/Z case), and 220 GeV when $m_{\tilde{\chi}_2^0} - m_{\tilde{\chi}_1^0} = 15$ GeV (the extreme off-shell W/Z case). By contrast, $\tilde{\chi}_2^0$ was excluded only up to a mass of 210 GeV for the off-shell W/Z case of the higgsino scenario, which occurred when $m_{\tilde{\chi}_2^0} - m_{\tilde{\chi}_1^0} = 10$ GeV or $m_{\tilde{\chi}_2^0} - m_{\tilde{\chi}_1^0} \gtrsim 35$ GeV.

- **ATLAS-1911-12606** [124]: Concentration on compressed mass spectra case and search for electroweakino pair or slepton pair production, with two leptons and missing transverse momentum as the final state. The results were projected onto the $\Delta m - \tilde{\chi}_2^0$ plane, where $\Delta m \equiv m_{\tilde{\chi}_2^0} - m_{\tilde{\chi}_1^0}$ for the electroweakino production. It was found that the tightest bound on the higgsino-dominated $\tilde{\chi}_2^0$ was 193 GeV in mass for $\Delta m \simeq 9.3$ GeV, and the optimum bound on the wino-dominated $\tilde{\chi}_2^0$ was 240 GeV in mass when $\Delta m \simeq 7$ GeV. Similarly, it was found that light-flavor sleptons should be heavier than about 250 GeV for $\Delta m_{\tilde{\ell}} = 10$ GeV, where $m_{\tilde{\ell}} \equiv m_{\tilde{\ell}} - m_{\tilde{\chi}_1^0}$.

Note that all the analyses were based on 139 fb⁻¹ data except for the second analysis, which studied 36 fb⁻¹ data.

3 Combined experimental impacts on MSSM

This research utilized the package **SARAH-4.14.3** [130–133] to build the model file of the MSSM, the codes **SPheno-4.0.4** [134, 135] and **FlavorKit** [136] to generate particle mass spectra and compute low energy observables, such as a_μ^{SUSY} and B-physics observables, and the package **MicrOMEGAs-5.0.4** [137–142] to calculate DM observables, assuming that the lightest neutralino was the sole DM candidate in the universe. Bounds from the direct search for extra Higgs bosons at the LEP, Tevatron, and LHC and the fit of h ’s property to LHC Higgs data were implemented by the programs **HiggsBounds-5.3.2** [143–146] and **HiggsSignal-2.2.3** [147–150], respectively.

3.1 Research strategy

The main aims of this research were to explore as many possibilities (parameter points) of the MSSM as possible, clarify how they remain consistent with current experimental results, and reveal some distinct characteristics of the theory. We carried out such research by the following procedures:

- We employed the **MultiNest** algorithm [151] to comprehensively scan the parameter space in Table 3. The n_{live} parameter in the algorithm controlled the number of active points sampled in each iteration of the scan, and $n_{\text{live}} = 10000$ was set. The following likelihood function was constructed to guide the scan:

$$\mathcal{L} = \mathcal{L}_{a_\mu} \times \mathcal{L}_{\text{const}}. \quad (3.1)$$

\mathcal{L}_{a_μ} is the likelihood function of the muon $g - 2$ anomaly given by

$$\mathcal{L}_{a_\mu} \equiv \text{Exp} \left[-\frac{1}{2} \left(\frac{a_\mu^{\text{SUSY}} - \Delta a_\mu}{\delta a_\mu} \right)^2 \right] = \text{Exp} \left[-\frac{1}{2} \left(\frac{a_\mu^{\text{SUSY}} - 2.51 \times 10^{-9}}{5.9 \times 10^{-10}} \right)^2 \right],$$

where $\Delta a_\mu \equiv a_\mu^{\text{Exp}} - a_\mu^{\text{SM}}$ and δa_μ denote the difference between the experimental central value of a_μ and its SM prediction and the total uncertainties in determining Δa_μ , respectively [8–30]. $\mathcal{L}_{\text{const}}$ represents the restrictions of some experiments on the theory. They included 2σ bounds of the DM relic density [152], upper bounds of the PandaX-4T experiment on the SI DM-nucleon scattering [107] and the XENON-1T experiment on the SD scattering [153], consistency of h ’s properties with the LHC Higgs data at the 95% confidence level [150], collider searches for extra Higgs bosons [146], 2σ bounds on the branching ratios of $B \rightarrow X_s \gamma$ and $B_s \rightarrow \mu^+ \mu^-$ [154], and the vacuum stability of the scalar potential consisting of the Higgs fields and the last two generations of slepton fields [155, 156]. We defined $\mathcal{L}_{\text{const}} = 1$ if the restrictions were satisfied and $\mathcal{L}_{\text{const}} = \text{Exp}[-100]$ if they were not. More details of these restrictions are introduced in Refs. [72, 86].

- We refined the samples obtained in the scan by the criteria $\mathcal{L}_{const} = 1$ and $|a_\mu^{\text{SUSY}} - \Delta a_\mu|/\delta a_\mu \leq 3$, and we projected those passing the selection onto the two-dimensional planes spanned by any two of the parameters M_1 , M_2 , μ , $\tilde{m}_{\tilde{\mu}_L}$, and $\tilde{m}_{\tilde{\mu}_R}$. We then concentrated on the region of the planes where the samples were sparsely distributed and performed a new scan by adjusting relevant parameter ranges and setting $n_{\text{live}} = 3000$.
- We iterated the last operation with all accumulated samples until the projected areas on the planes remained unchanged. At this point, we acquired 2.21×10^5 samples surviving the criteria, and about 1.7×10^5 of them could further explain the $(g-2)_\mu$ anomaly at the 2σ level.
- We simplified the study of the restrictions from the LHC search for SUSY. Specifically, given that the sample number was huge and the Monte Carlo simulation of each sample introduced below would cost more than one core-hour for our computing cluster, we selected some representative points and carried out the simulations. These points were stored in a specially designed sample database, achieved in the following way:
 1. We searched for the sample with the greatest likelihood value from a database storing all the scan results.
 2. We constructed a hypersphere in the parameter space, which was centered around the sample with a radius of 10 GeV for M_1 , M_2 , and μ (note that the simulation results were more sensitive to these three parameters than the other dimensional parameters), 20 GeV for $\tilde{m}_{\tilde{\mu}_L}$ and $\tilde{m}_{\tilde{\mu}_R}$, and one unit for $\tan \beta$.
 3. We copied useful information of the central sample to the newly built database for simulation and sequentially deleted all samples in the hypersphere to update the initial database.
 4. We iterated the above operations until all the samples in the initial database were depleted.

We add that the method to dilute the dense samples was plausible because the R-value of the simulation relied heavily on both the mass spectra and the field compositions of sparticles, which determined their production cross sections and decay branching ratios. All samples in the hypersphere had similar properties in these two aspects, and the R-value of the studied point was typical for these samples. In addition, the method paid more attention to the samples favored by the anomaly, which was the focus of this research. After requiring the representative points to explain the muon g-2 anomaly at the 2σ level, we finally acquired 58242 samples for the simulations.

- We surveyed the LHC restrictions on the representative points by simulating the following processes:

$$pp \rightarrow \tilde{\chi}_i^0 \tilde{\chi}_j^\pm, \quad i = 2, 3, 4, 5, \quad j = 1, 2; \quad (3.2)$$

$$pp \rightarrow \tilde{\chi}_i^\pm \tilde{\chi}_j^\mp, \quad i, j = 1, 2; \quad (3.3)$$

$$pp \rightarrow \tilde{\chi}_i^0 \tilde{\chi}_j^0, \quad i, j = 2, 3, 4, 5; \quad (3.4)$$

$$pp \rightarrow \tilde{\mu}_i^* \tilde{\mu}_j, \quad i, j = 1, 2; \quad (3.5)$$

$$pp \rightarrow \tilde{\nu}_\mu^* \tilde{\nu}_\mu. \quad (3.6)$$

Specifically, the cross sections of these processes at $\sqrt{s} = 13$ TeV were calculated at the next-to-leading order (NLO) by the package `Prospino2` [157], and 60000 and 40000 events were generated for the electroweakino and slepton production processes, respectively, by the package `MadGraph_aMC@NLO` [158, 159]. A relevant parton shower and hadronization were completed by the program `PYTHIA8` [160]. The resulting event files were then fed into the package `CheckMATE-2.0.29` [161–163] to calculate the R -value defined by $R \equiv \max\{S_i/S_{i,obs}^{95}\}$, where S_i denotes the simulated event number of the i -th SR in the analyses of Tables 1 and 2, and $S_{i,obs}^{95}$ represents its corresponding 95% confidence level upper limit. In this process, program `Delphes` was encoded in `CheckMATE` for detector simulation [164].

As an alternative, we also used the program `SModelS-2.2.1` [165] to study the LHC restrictions. We found that this program’s capability to exclude SUSY points was usually weaker than that of the simulation due to its limited database and strict working prerequisites.

3.2 Key features of the results

First, we studied the DM physics of the MSSM by projecting the samples acquired by the scans onto the $M_1 - M_2$ and $M_1 - \mu$ planes to obtain Fig. 1. This figure reveals the following facts:

- If only the restrictions from the DM physics are considered, the DM candidate is bino-dominated when $|M_1| \leq 800$ GeV. It may achieve the measured relic density by Z-mediated resonant annihilation, h -mediated resonant annihilation, or co-annihilation with wino-like electroweakinos. In addition, we will show later in Figs. 5 and 6 that it may also acquire the density by co-annihilating with $\tilde{\mu}_L/\tilde{\nu}_\mu$ or $\tilde{\mu}_R$.
- If the samples are further required to explain the muon g-2 anomaly at the 2σ level, $|M_1|$ is upper bounded by about 620 GeV. Furthermore, if the LHC restrictions are included, it is upper bounded by about 570 GeV.

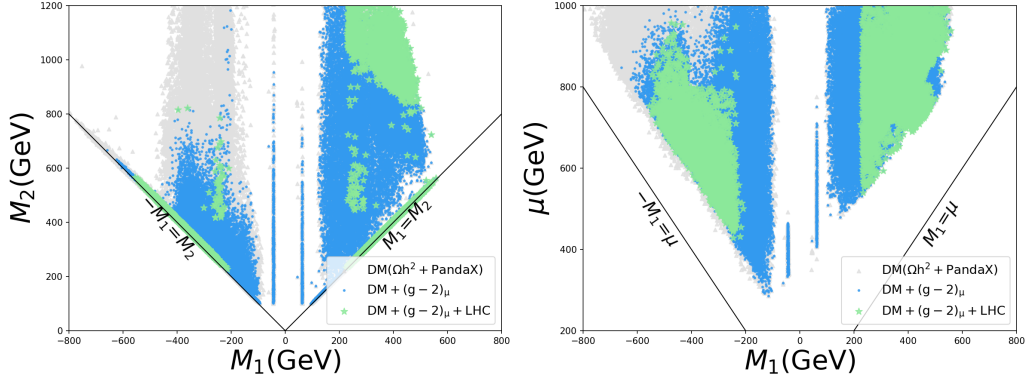


Figure 1. Projection of the obtained samples onto $M_1 - M_2$ plane (left panel) and $M_1 - \mu$ plane (right panel). The gray triangles denote the samples that satisfy all restrictions listed in the text, in particular those from the DM relic density measured by the Planck experiment [152] and the DM direct detection of the PandaX-4T experiment [107]. The blue circles represent those that could further explain the muon g-2 anomaly at the 2σ level, and the green stars are the part of the blue circles that agree with the results from the LHC search for SUSY. Although only about one-third of the blue circles were studied by the simulations in this work (see the research strategy in the last sub-section), the shape of the green areas is unlikely to significantly change. We verified this point by randomly selecting several thousands of samples from the blue areas and simulating the LHC restrictions.

- There is a vacant region on the $M_1 - M_2$ plane, located in the ranges of $350 \text{ GeV} \lesssim M_1 \lesssim 570 \text{ GeV}$, $400 \text{ GeV} \lesssim M_2 \lesssim 600 \text{ GeV}$, and $M_1 + 30 \text{ GeV} \lesssim M_2 \lesssim M_1 + 100 \text{ GeV}$. This region is distinct because winos can significantly affect the mass of $\tilde{\nu}_\mu$ by radiative corrections, and given the values of M_1 and M_2 , one needs to fine-tune the soft-breaking parameter $\tilde{m}_{\tilde{\mu}_L}$ to predict the measured DM density by the co-annihilation with $\tilde{\nu}_\mu/\tilde{\mu}_L$. This situation is challenging in the scans since it easily results in $\tilde{\nu}_\mu$ as the LSP.

We add that this vacant region corresponds to the void on the bottom right corner of the $|m_{\tilde{\chi}_1^0}| - m_{\tilde{\chi}_1^\pm}$ plane in Fig. 4.

- The PandaX-4T experiment has required $\mu \gtrsim 300 \text{ GeV}$ when M_1 is negative and $\mu \gtrsim 500 \text{ GeV}$ if $M_1 > 100 \text{ GeV}$. This conclusion originates from the facts that $m_{\tilde{\chi}_1^0} \simeq M_1$ and the formulae of $\sigma_{\tilde{\chi}_1^0-N}^{\text{SI}}$ in Eqs. 2.2 and 2.4. This explains why μ at $M_1 \simeq -m_Z/2$ may be much smaller than μ at $M_1 \simeq m_Z/2$.
- The observables in the DM physics and the muon g-2 anomaly may prefer different parameter spaces of the MSSM, even though broad parameter regions can still accommodate both. For example, a negative M_1 is disfavored by the muon g-2 anomaly in the large μ and M_2 region, because the ‘BLR’ contribution to a_μ^{SUSY} is negatively sizable. This case, however, can easily reproduce the results of DM experiments.

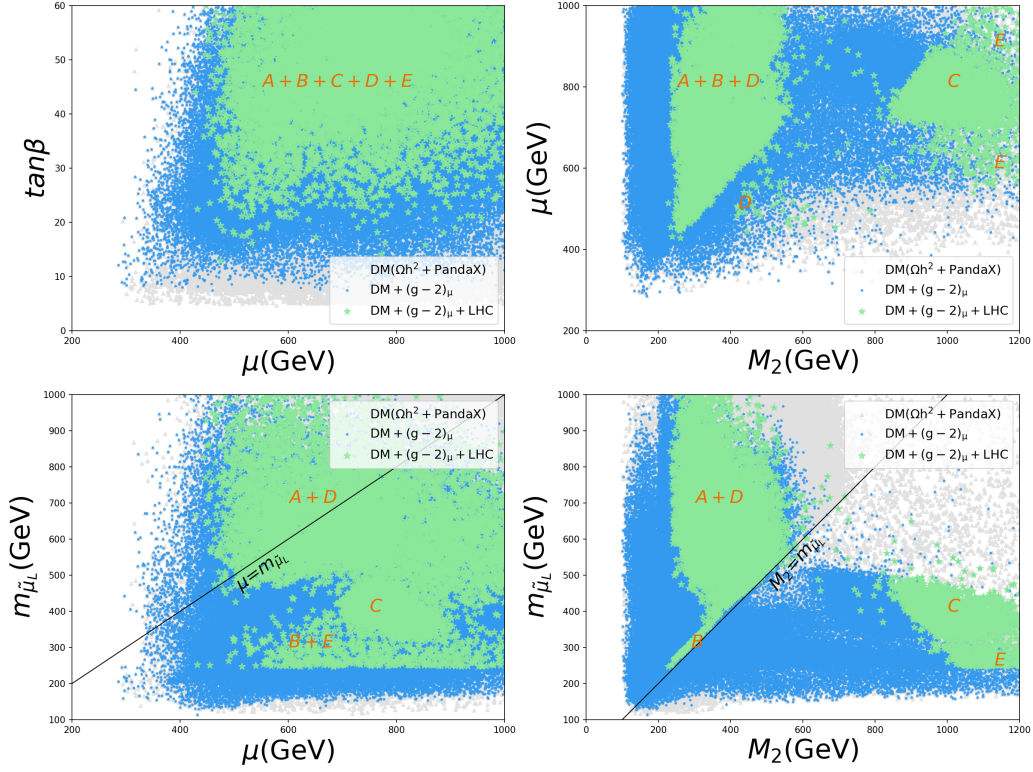


Figure 2. Similar to Fig. 1, but showing the correlations of the parameters that a_μ^{SUSY} is sensitive to. $m_{\tilde{\mu}_L}$ is the mass of the left-handed-dominated smuon, which is approximately equal to the soft-breaking parameter $\tilde{m}_{\tilde{\mu}_L}$ at the slepton mass scale. Samples surviving the LHC restrictions are classified into five types, marked by A, B, C, D, and E in this figure. They are distinguished by different DM annihilation mechanisms and locations in the SUSY parameter space (see Table 4).

Table 4. Parameter spaces for the five types of samples in Fig. 2, where the theoretical inputs in the last five columns are in units of GeV. The second column denotes which particles $\tilde{\chi}_1^0$ will co-annihilate with to acquire the measured DM density. In this aspect, Type-A and Type-B samples are different in that $m_{\tilde{\mu}_L} \gtrsim M_2 + 30$ GeV for the former and $m_{\tilde{\mu}_L} \simeq M_2$ for the latter.

Sample type	Annihilation partner	M_1	M_2	μ	$m_{\tilde{\mu}_L}$	$m_{\tilde{\mu}_R}$
Type-A	\tilde{W}	(220, 560)	(230, 600)	(430, 1000)	(350, 1000)	(300, 1000)
Type-B	$\tilde{\mu}_L$ and \tilde{W}	(210, 550)	(230, 600)	(430, 1000)	(240, 600)	(300, 1000)
Type-C	$\tilde{\mu}_L$	(230, 540)	(600, 1400)	(540, 1000)	(240, 550)	(230, 1000)
Type-D	$\tilde{\mu}_R$	(210, 520)	(300, 700)	(440, 1000)	(400, 1000)	(210, 1000)
Type-E	$\tilde{\mu}_R$	(230, 320)	(950, 1300)	(570, 1000)	(240, 600)	(230, 1000)

Second, we concentrate on the interplay between the muon g-2 anomaly and the LHC restrictions. As introduced in the last section, explaining the muon g-2 anomaly requires more than one sparticle to be moderately light [84]. In particular, M_2 , μ , and $m_{\tilde{\mu}_L}$ can not be very large simultaneously since the ‘WHL’ contribution is

usually dominant. This situation leads to sizable SUSY signals and thus strengthens the LHC restrictions. In Fig. 2, we show the correlations of any two of the three parameters, M_2 , μ , and $m_{\tilde{\mu}_L}$, and also the correlation between μ and $\tan\beta$. The following distinct features are shown:

- The LHC restrictions have set lower bounds on the SUSY parameters: $\tan\beta \gtrsim 12$, $\mu \gtrsim 400$ GeV, $M_2 \gtrsim 230$ GeV, and $m_{\tilde{\mu}_L} \gtrsim 240$ GeV.
- As indicated by the top left panel, the LHC restrictions are particularly strong for $\tan\beta \lesssim 25$. The underlying reason is the muon g-2 anomaly prefers light winos, higgsinos, and left-handed-dominant smuon as $\tan\beta$ becomes small.
- In the case that $\tilde{\mu}_L$ is lighter than winos and/or higgsinos, the LHC restrictions are also strong, which is reflected by the wedge-shaped excluded regions on the $M_2 - m_{\tilde{\mu}_L}$ and $\mu - m_{\tilde{\mu}_L}$ planes. This was because the heavy electroweakinos could decay into the slepton first and thus enhance the leptonic signal of the electroweakino pair production processes (compared with the case where $\tilde{\mu}_L$ is heavier than the electroweakinos). We elaborate on this point by fixing $m_{\tilde{\mu}_L} = 300$ GeV and varying M_2 . For $M_2 \simeq 300$ GeV, although the total wino pair production cross sections exceeded 550 fb [166, 167], there were some samples surviving the LHC constraints due to the small mass splittings between the wino-like particles and $\tilde{\chi}_1^0$. In this case, the wino-like particles decayed into $\tilde{\chi}_1^0$ and a soft virtual Z or W, which made the signal detection difficult. With the increase in M_2 , all the samples were excluded because the wino-like particles were copiously produced at the LHC due to their moderate lightness, and simultaneously the branching ratios of their decays into the slepton were sizable. Specifically, we found that the ratios were always larger than 20%. With the further increase in M_2 , the wino pair production rates rapidly decreased so that the LHC constraints were weakened, reflected by the appearance of the green areas at $M_2 \simeq 900$ GeV in the bottom right panel. We add that this discussion can be applied to the $\mu - m_{\tilde{\mu}_L}$ plane in the bottom left panel.
- Samples consistent with the LHC restrictions can be classified into five types, distinguished by their DM annihilation mechanisms and locations in the parameter space. They are marked as A, B, C, D, and E in the figure. In Table 4, we provide the criteria of this classification. We will present benchmark points to reveal their properties and study the LHC restrictions later.

Third, we studied the impact of the LZ experiment on the MSSM. In Figs. 1 and 2, the PandaX-4T results were used to set upper bounds on the SI cross sections of the DM-nucleon scattering [107]. We utilized the LZ limits to refine the samples further, project the selected samples onto various panels, and compare the resulting figures with their correspondence plotted with the samples in Fig. 1. The most

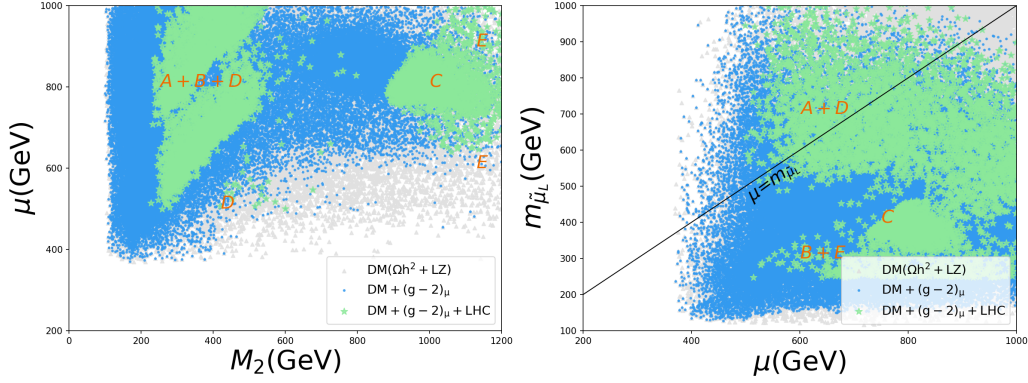


Figure 3. Left panel: same as the upper right panel of Fig. 2, except that all the samples are required further to satisfy the LZ restrictions. Right panel: same as the left panel of this figure, except that the samples are projected onto the $\mu - m_{\tilde{\mu}_L}$ plane.

Table 5. Numbers of the samples studied by the simulations. They are categorized by DM-dominant annihilation mechanisms, where a DM direct detection experiment is used to set the limits, and whether the LHC restrictions are included in the research.

Annihilation Mechanisms	Before LHC Constraints		After LHC Constraints	
	PandaX	LZ	PandaX	LZ
Total Samples	58242	39657	11204	5656
$\tilde{B} - \tilde{W}$ co-annihilation	31108	20123	7927	3435
$\tilde{B} - \tilde{\mu}_L - \tilde{W}$ co-annihilation	10052	6622	287	174
$\tilde{B} - \tilde{\mu}_L$ co-annihilation	13445	11052	2737	1884
$\tilde{B} - \tilde{\mu}_R$ co-annihilation	2869	1860	253	163
Z - funnel	408	0	0	0
h - funnel	360	0	0	0

remarkable change was that μ was more strongly limited, which was reflected in the following aspects.

- Given the measured DM density, the LZ experiment alone required $\mu \gtrsim 380$ GeV for $M_1 < 0$ and $\mu \gtrsim 600$ GeV for $M_1 > 100$ GeV. If the restrictions from the muon $g-2$ anomaly and the LHC experiment were also included, the lower bounds became about 500 GeV and 630 GeV, respectively, indicating that the theory needs a tuning of $\mathcal{O}(1\%)$ to predict the Z -boson mass [168]. Compared with the restriction from the PandaX-4T experiment, these bounds were improved by about 100 GeV.
- The Z -mediated resonant annihilation becomes less favored because an enhanced μ reduced $C_{\tilde{\chi}_1^0 \tilde{\chi}_1^0 Z}$ in Eq. 2.5, and $2|m_{\tilde{\chi}_1^0}|$ must be closer to m_Z to obtain the measured density. This situation requires the fine-tuning quantity defined

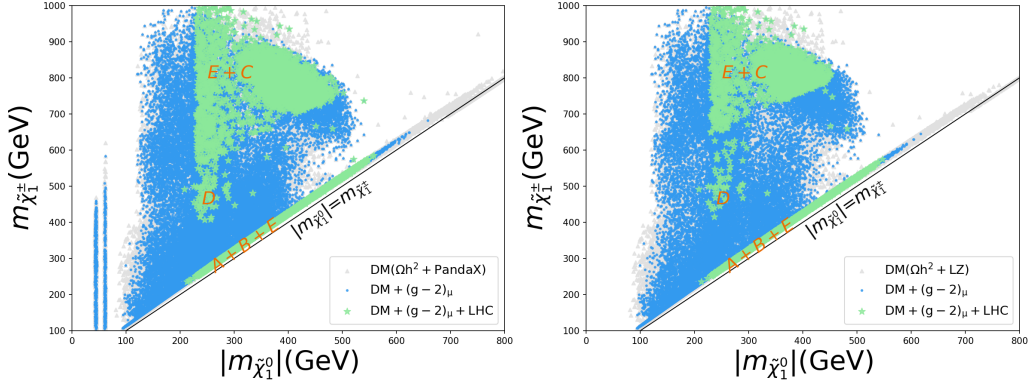


Figure 4. Distribution of $m_{\tilde{\chi}_1^\pm}$ versus $|m_{\tilde{\chi}_1^0}|$. The left panel studies the samples in Figs. 1, while the right panel focuses on those in Fig. 3. The classification in Table 4 is applied to the samples of this figure to illuminate the underlying physics.

in Eq. (19) of Ref. [169] to be larger than about 150 to achieve the measured density. This conclusion also applies to the h -mediated resonant annihilation. We point out that, due to the tuning, these resonant annihilation scenarios were usually missed in the scans (see, e.g., the results in Fig. 4 of this study). This point was discussed with Bayesian statistics in footnote 6 of Ref. [89].

- Since the LZ constraint and the LHC restriction are sensitive to different SUSY parameters, they complement each other in exploring the features of the MSSM. This is particularly so if one intends to explain the muon $g-2$ anomaly at the 2σ level. The basic reason is that μ is correlated with the other parameters by the anomaly, and any enhancement of μ in a massive higgsino scenario will make winos and $\tilde{\mu}_L$ lighter to keep a_μ^{SUSY} unchanged. This situation usually improves the LHC restrictions.

To show the combined effects, we projected the samples passing the LZ restrictions onto the $M_2 - \mu$ and $\mu - m_{\tilde{\mu}_L}$ planes in Fig. 3 and compared the resulting panels with their corresponding ones in Fig. 2. We also focused on the samples studied by the Monte Carlo simulations. We classified them by DM-dominant annihilation mechanisms, where the DM experiment was used to set limits, and whether the LHC restrictions are included in this research, and the results are presented in Table 5. Both the figure and the table show that the two experiments promoted each other to limit the parameter space of the MSSM.

Fourth, we surveyed the influences of these experiments on the particle properties. We projected the samples of Fig. 1 (Fig. 3) onto the $|m_{\tilde{\chi}_1^0}| - m_{\tilde{\chi}_1^\pm}$, $|m_{\tilde{\chi}_1^0}| - m_{\tilde{\mu}_L}$, and $|m_{\tilde{\chi}_1^0}| - m_{\tilde{\mu}_R}$ planes to acquire the left (right) panels of Figs. 4, 5, and 6, respectively. The classification of the samples was the same as before. From these plots, we obtained the following points:

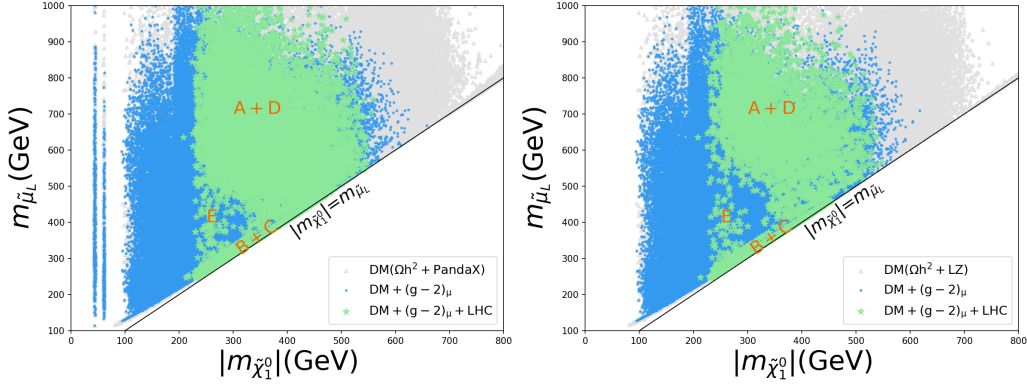


Figure 5. Same as Fig. 4 except that it shows the distribution on the $|m_{\tilde{\chi}_1^0}| - m_{\tilde{\mu}_L}$ plane.

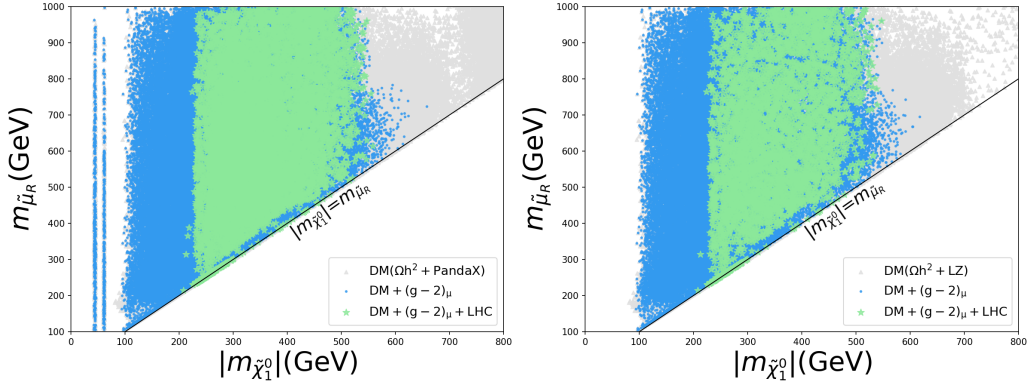


Figure 6. Same as Fig. 4 except that the samples are displayed on the $|m_{\tilde{\chi}_1^0}| - m_{\tilde{\mu}_R}$ plane.

- With the increase in $|m_{\tilde{\chi}_1^0}|$, the upper bounds of $m_{\tilde{\chi}_1^\pm}$ and $m_{\tilde{\mu}_L}$ decrease, and they terminate at $m_{\tilde{\chi}_1^\pm} \lesssim 600$ GeV and $m_{\tilde{\mu}_L} \lesssim 700$ GeV for $m_{\tilde{\chi}_1^\pm} \simeq 570$ GeV. This tendency is not evident for $m_{\tilde{\mu}_R}$ in the case of $m_{\tilde{\mu}_R} \leq 1$ TeV because a_μ^{SUSY} is more sensitive to M_2 , μ , and $m_{\tilde{\mu}_L}$ than to $m_{\tilde{\mu}_R}$, as indicated by Eqs. 2.6–2.9, and it decouples in the heavy sparticles limit.
- The LHC restrictions have set lower bounds on the sparticle mass spectra, which were $m_{\tilde{\chi}_1^0} \gtrsim 210$ GeV, $m_{\tilde{\chi}_1^\pm} \gtrsim 235$ GeV, $m_{\tilde{\mu}_L} \gtrsim 240$ GeV, and $m_{\tilde{\mu}_R} \gtrsim 215$ GeV in this research. The basic reason for this phenomenon is as follows: if $\tilde{\chi}_1^0$ is lighter, more missing momentum will be emitted in the sparticle production processes at the LHC, which can improve the sensitivities of the experimental analyses; however, if sparticles other than $\tilde{\chi}_1^0$ are lighter, they will be more copiously produced at the LHC to increase the number of events containing multiple leptons. We emphasize that these bounds should be regarded as rough estimates, instead of accurate values, since far from enough samples were studied, given the broad parameter space of the MSSM.

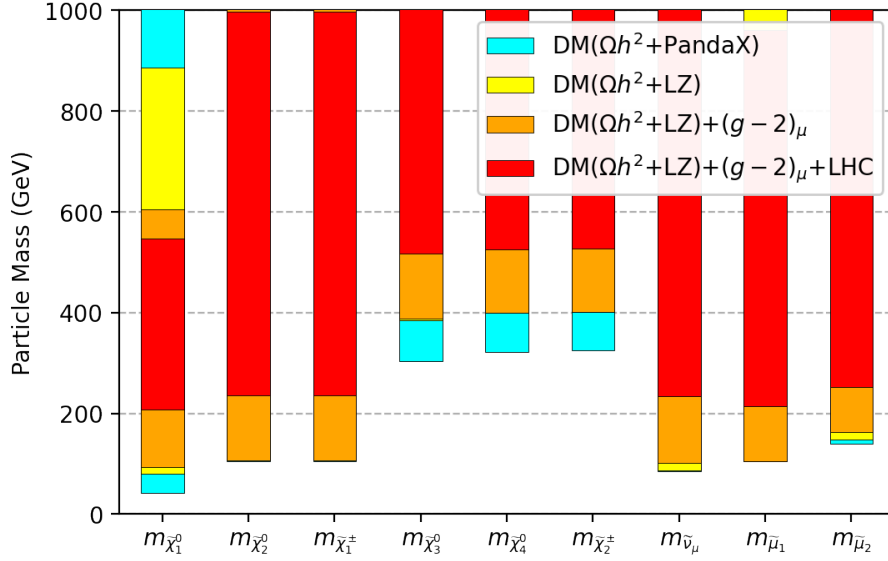


Figure 7. Sparticle mass spectra preferred by different experiments. The cyan band is acquired from the gray samples in Fig. 1, and the yellow, orange, and red bands are from the gray, blue, and green samples in Fig. 3, respectively.

Finally, we summarize the sparticle mass spectra preferred by different experiments in Fig. 7. This figure reveals that $570 \text{ GeV} \gtrsim m_{\tilde{\chi}_1^0} \gtrsim 210 \text{ GeV}$, $m_{\tilde{\chi}_2^0}, m_{\tilde{\chi}_1^\pm} \gtrsim 235 \text{ GeV}$, $m_{\tilde{\chi}_3^0} \gtrsim 515 \text{ GeV}$, $m_{\tilde{\chi}_4^0} \gtrsim 525 \text{ GeV}$, $m_{\tilde{\chi}_2^\pm} \gtrsim 530 \text{ GeV}$, $m_{\tilde{\nu}_\mu} \gtrsim 235 \text{ GeV}$, $950 \text{ GeV} \gtrsim m_{\tilde{\mu}_1} \gtrsim 215 \text{ GeV}$, and $m_{\tilde{\mu}_2} \gtrsim 250 \text{ GeV}$ if all the latest restrictions are considered. The lower bounds come from the LHC restrictions, and the upper bounds arise from the explanation of the muon $g-2$ anomaly at the 2σ level. In addition, it is verified that $\tilde{\chi}_2^0$ and $\tilde{\chi}_1^\pm$ are wino-dominated when they are lighter than about 500 GeV and $m_{\tilde{\mu}_1}$ may be either $m_{\tilde{\mu}_L}$ or $m_{\tilde{\mu}_R}$. It was also verified that $600 \text{ GeV} \gtrsim m_{\text{NLSP}} \gtrsim 220 \text{ GeV}$ and $700 \text{ GeV} \gtrsim m_{\text{NNLSP}} \gtrsim 250 \text{ GeV}$, where the NLSP and NNLSP may be either electroweakinos or sleptons. In principle, the sparticles other than $\tilde{\chi}_1^0$ and $\tilde{\mu}_1^0$ are also upper bounded in mass by the explanation of the anomaly. We do not provide these bounds since the parameter space in Table 3 is limited.

3.3 More details of LHC restrictions

Even in the simple realization of SUSY, such as the MSSM, the decay products of heavy sparticles are complex (see the benchmark points presented below). As a result, the pair productions of winos, higgsinos, $\tilde{\mu}_L$, and $\tilde{\mu}_R$ at the LHC, $pp \rightarrow \tilde{W}\tilde{W}, \tilde{H}\tilde{H}, \tilde{\mu}_L^*\tilde{\mu}_L, \tilde{\mu}_R^*\tilde{\mu}_R$, may contribute to the same SR of the analyses in Tables 1 and 2. All these contributions must be suppressed for any parameter point to circumvent the LHC restrictions, which may occur in the following situations:

Table 6. Supplement to Table 5 with the SRs that contribute to the largest R-values and their capability to exclude the samples, expressed by the percentage of the total numbers in the second column. This table only counts the samples satisfying the LZ restrictions and studied by the simulations. The second and third columns denote the sample numbers before and after implementing the LHC restrictions, respectively, which are also presented in Table 5. They reflect that the LHC restrictions on the $\tilde{B} - \tilde{\mu}_L - \tilde{W}$ and $\tilde{B} - \tilde{\mu}_R$ co-annihilation cases are very strong. One can understand this feature from the previous discussions in this research and the benchmark points listed below. The fourth column reveals that only SR-1 from the experimental analyses in Ref. [6] and SR-2 from Ref. [113, 114] played a role in excluding the $\tilde{B} - \tilde{\mu}_L$ co-annihilation case, which was different from the other cases.

Annihilation mechanism	Before	After	SRs and their exclusion percentages
Total samples	39657	5656	SR-1(23.7%),SR-2(18.5%),SR-3(12.7%),SR-4(11.6%)
$\tilde{B} - \tilde{W}$ co-annihilation	20123	3435	SR-3(23.8%), SR-4(21.1%), SR-5(6.3%), SR-1(0.1%)
$\tilde{B} - \tilde{\mu}_L - \tilde{W}$ co-annihilation	6622	174	SR-3(28.6%),SR-4(16.4%),SR-2(14.4%),SR-5(11.7%)
$\tilde{B} - \tilde{\mu}_L$ co-annihilation	11052	1884	SR-1(52.0%),SR-2(30.4%)
$\tilde{B} - \tilde{\mu}_R$ co-annihilation	1860	163	SR-2(44.0%), SR-4(32.3%), SR-3(6.2%), SR-1(0.8%)

1. The DM candidate is massive, compared with the results of pertinent experimental analyses. In this case, all SM particles in the final state are not energetic enough, and the missing momentum emitted in the sparticle production processes tends to be small.
2. The mass splitting between the decaying sparticle and $\tilde{\chi}_1^0$ is less than several tens of GeV. In this compressed spectra case, the SM particles as the decay product are soft and hard to detect without a deliberate search strategy.
3. Heavy sparticles decay by several channels with comparable branching ratios in terms of size. This situation usually leads to complicated final decay states.
4. Sparticles are sufficiently heavy, compared with their experimental exclusion bounds in simplified models, so that their production cross sections are negligibly small.

We refer to these situations as survival mechanisms I, II, III, and IV in the following discussion. An illuminating example of situations 1 and 2 is presented in Fig. 16 of Ref. [112], which concludes that there are no LHC restrictions on winos in the $\tilde{B} - \tilde{W}$ co-annihilation case if $m_{\tilde{\chi}_1^0} \gtrsim 220$ GeV. Evidently, this bound is significantly weaker than the other searches for winos at the LHC.

To simplify the discussion of the LHC restrictions, we first classify the blue samples in Fig. 3 by DM annihilation mechanisms, similar to what we did in Table 5. Then, we only focused on the samples studied by the Monte Carlo simulations. We show in Table 6 the numbers before and after simulating the LHC restrictions, the

Table 7. Two benchmark points, P1 and P2, for Type-A and -B samples in Table 4, respectively. Both points satisfy all the restrictions listed in the text. The R-value of each point and its corresponding SR are presented in the last line of this table.

Benchmark Point P1 for Type-A samples				Benchmark Point P2 for Type-B samples			
μ	750.7 GeV	m_H	10359.8 GeV	μ	636.8 GeV	m_H	7359.7 GeV
$\tan\beta$	53.2	m_A	10359.8 GeV	$\tan\beta$	35.5	m_A	7359.7 GeV
A_t	2496.8 GeV	m_h	125.5 GeV	A_t	2409.8 GeV	m_h	125.2 GeV
M_1	-380.0 GeV	m_{H^\pm}	10337.7 GeV	M_1	-292.9 GeV	m_{H^\pm}	7363.2 GeV
M_2	386.9 GeV	$m_{\tilde{\nu}_\mu}$	678.0 GeV	M_2	304.9 GeV	$m_{\tilde{\nu}_\mu}$	316.2 GeV
$\tilde{m}_{\tilde{u}_L}$	550.2 GeV	$m_{\tilde{\chi}_1^0}$	-380.7 GeV	$\tilde{m}_{\tilde{u}_L}$	188.4 GeV	$m_{\tilde{\chi}_1^0}$	-292.7 GeV
$\tilde{m}_{\tilde{u}_R}$	972.5 GeV	$m_{\tilde{\chi}_2^0}$	404.8 GeV	$\tilde{m}_{\tilde{u}_R}$	708.0 GeV	$m_{\tilde{\chi}_2^0}$	317.4 GeV
$\tilde{m}_{\tilde{d}_L}$	682.2 GeV	$m_{\tilde{\chi}_3^0}$	-772.6 GeV	$\tilde{m}_{\tilde{d}_L}$	325.6 GeV	$m_{\tilde{\chi}_3^0}$	-656.4 GeV
$\tilde{m}_{\tilde{d}_R}$	806.5 GeV	$m_{\tilde{\chi}_4^0}$	777.7 GeV	$\tilde{m}_{\tilde{d}_R}$	612.9 GeV	$m_{\tilde{\chi}_4^0}$	662.0 GeV
a_μ^{SUSY}	1.95×10^{-9}	$m_{\tilde{\chi}_1^\pm}$	405.0 GeV	a_μ^{SUSY}	2.43×10^{-9}	$m_{\tilde{\chi}_1^\pm}$	317.6 GeV
Ωh^2	0.10	$m_{\tilde{\chi}_2^\pm}$	779.6 GeV	Ωh^2	0.12	$m_{\tilde{\chi}_2^\pm}$	664.2 GeV
σ_p^{SI}	$4.50 \times 10^{-47} \text{cm}^2$	σ_p^{SD}	$5.38 \times 10^{-43} \text{cm}^2$	σ_p^{SI}	$4.34 \times 10^{-47} \text{cm}^2$	σ_p^{SD}	$9.21 \times 10^{-43} \text{cm}^2$
$N_{11}, N_{12}, N_{13}, N_{14}$	-0.997, -0.004, -0.075, -0.036			$N_{11}, N_{12}, N_{13}, N_{14}$	-0.996, -0.004, -0.083, -0.036		
$N_{21}, N_{22}, N_{23}, N_{24}$	0.004, 0.987, -0.140, 0.075			$N_{21}, N_{22}, N_{23}, N_{24}$	0.006, 0.985, -0.157, 0.079		
$N_{31}, N_{32}, N_{33}, N_{34}$	0.079, -0.046, -0.702, -0.706			$N_{31}, N_{32}, N_{33}, N_{34}$	0.084, -0.055, -0.700, -0.707		
$N_{41}, N_{42}, N_{43}, N_{44}$	-0.027, 0.152, 0.694, -0.703			$N_{41}, N_{42}, N_{43}, N_{44}$	-0.033, 0.166, 0.691, -0.702		
Annihilations	Fractions[%]			Annihilations	Fractions[%]		
$\bar{B} - \bar{W}$ Co-annihilation	89.9			$\bar{B} - \bar{W}/\bar{B} - \bar{\mu}_L$ Co-annihilation	73.0/14.5		
Decays	Branching ratios[%]			Decays	Branching ratios[%]		
$\tilde{\chi}_2^0 \rightarrow \tilde{\chi}_1^0 Z^*/\tilde{\chi}_1^0 h^*$	100			$\tilde{\chi}_2^0 \rightarrow \tilde{\nu}_\mu \nu_\mu$	100		
$\tilde{\chi}_3^0 \rightarrow \tilde{\chi}_1^\pm W^\mp/\tilde{\chi}_2^0 Z/\tilde{\chi}_1^0 h/\tilde{\chi}_2^0 h/\tilde{\chi}_1^0 Z$	61.0/27.0/8.3/2.3/1.1			$\tilde{\chi}_3^0 \rightarrow \tilde{\chi}_1^\pm W^\mp/\tilde{\chi}_2^0 Z/\tilde{\chi}_1^0 h/\tilde{\chi}_2^0 h/\tilde{\chi}_1^0 Z$	61.2/26.4/7.7/2.6/1.4		
$\tilde{\chi}_4^0 \rightarrow \tilde{\chi}_1^\pm W^\mp/\tilde{\chi}_2^0 h/\tilde{\chi}_1^0 Z/\tilde{\chi}_2^0 Z/\tilde{\chi}_1^0 h$	61.3/26.2/8.3/2.8/1.0			$\tilde{\chi}_4^0 \rightarrow \tilde{\chi}_1^\pm W^\mp/\tilde{\chi}_2^0 h/\tilde{\chi}_1^0 Z/\tilde{\chi}_2^0 Z/\tilde{\nu}_\mu \nu_\mu/\tilde{\chi}_1^0 h/\tilde{\mu}_L^\pm \mu^\mp$	60.9/24.7/7.6/3.3/1.4/1.2/0.9		
$\tilde{\chi}_1^\pm \rightarrow \tilde{\chi}_1^0 (W^\pm)^*$	100			$\tilde{\chi}_1^\pm \rightarrow \tilde{\nu}_\mu \mu^\pm$	99.9		
$\tilde{\chi}_2^\pm \rightarrow \tilde{\chi}_2^0 W^\pm/\tilde{\chi}_1^\pm Z/\tilde{\chi}_1^\pm h/\tilde{\chi}_1^0 W^\pm$	31.0/30.1/28.6/9.9			$\tilde{\chi}_2^\pm \rightarrow \tilde{\chi}_2^0 W^\pm/\tilde{\chi}_1^\pm Z/\tilde{\chi}_1^\pm h/\tilde{\chi}_1^0 W^\pm/\tilde{\mu}_L^\pm \nu_\mu/\tilde{\nu}_\mu \mu^\pm$	30.8/29.7/27.4/9.6/1.9/0.6		
$\tilde{\mu}_L^\pm \rightarrow \tilde{\chi}_1^\pm \nu_\mu/\tilde{\chi}_2^0 \mu^\pm/\tilde{\chi}_1^0 \mu^\pm$	58.8/30.0/11.2			$\tilde{\mu}_L^\pm \rightarrow \tilde{\chi}_1^0 \mu^\pm/\tilde{\chi}_1^\pm \nu_\mu/\tilde{\chi}_2^0 \mu^\pm$	63.4/23.7/12.9		
$\tilde{\mu}_R^\pm \rightarrow \tilde{\chi}_1^0 \mu^\pm/\tilde{\nu}_\mu W^\pm$	99.8/0.1			$\tilde{\mu}_R^\pm \rightarrow \tilde{\chi}_1^0 \mu^\pm/\tilde{\nu}_\mu W^\pm/\tilde{\mu}_L^\pm h/\tilde{\mu}_L^\pm Z$	99.5/0.3/0.1/0.1		
$\tilde{\nu}_\mu \rightarrow \tilde{\chi}_1^\pm \mu^\mp/\tilde{\chi}_2^0 \nu_\mu/\tilde{\chi}_1^0 \nu_\mu$	59.8/29.4/10.8			$\tilde{\nu}_\mu \rightarrow \tilde{\chi}_1^0 \nu_\mu$	100		
R value	0.37, S-high-mm-05 in SR-3			R value	0.30, SRG07-0j_mll in SR-1		

Table 8. Same as Table 7, but for the benchmark points of Type-C and -D samples in Table 4, labeled as P3 and P4, respectively.

Benchmark Point P3 for Type-C samples				Benchmark Point P4 for Type-D samples			
μ	773.0 GeV	m_H	9252.5 GeV	μ	751.5 GeV	m_H	2738.6 GeV
$\tan\beta$	54.1	m_A	9252.5 GeV	$\tan\beta$	58.2	m_A	2738.6 GeV
A_t	2653.7 GeV	m_h	125.6 GeV	A_t	2485.9 GeV	m_h	125.4 GeV
M_1	360.6 GeV	m_{H^\pm}	9229.6 GeV	M_1	264.8 GeV	m_{H^\pm}	2766.4 GeV
M_2	1091.0 GeV	$m_{\tilde{\nu}_\mu}$	363.9 GeV	M_2	530.4 GeV	$m_{\tilde{\nu}_\mu}$	593.6 GeV
$\tilde{m}_{\tilde{u}_L}$	113.7 GeV	$m_{\tilde{\chi}_1^0}$	360.7 GeV	$\tilde{m}_{\tilde{u}_L}$	592.0 GeV	$m_{\tilde{\chi}_1^0}$	264.1 GeV
$\tilde{m}_{\tilde{u}_R}$	1274.6 GeV	$m_{\tilde{\chi}_2^0}$	785.0 GeV	$\tilde{m}_{\tilde{u}_R}$	263.0 GeV	$m_{\tilde{\chi}_2^0}$	545.0 GeV
$\tilde{m}_{\tilde{d}_L}$	372.0 GeV	$m_{\tilde{\chi}_3^0}$	-793.7 GeV	$\tilde{m}_{\tilde{d}_L}$	599.2 GeV	$m_{\tilde{\chi}_3^0}$	-769.1 GeV
$\tilde{m}_{\tilde{d}_R}$	1187.7 GeV	$m_{\tilde{\chi}_4^0}$	1136.1 GeV	$\tilde{m}_{\tilde{d}_R}$	268.5 GeV	$m_{\tilde{\chi}_4^0}$	782.4 GeV
a_μ^{SUSY}	1.99×10^{-9}	$m_{\tilde{\chi}_1^\pm}$	784.3 GeV	a_μ^{SUSY}	2.33×10^{-9}	$m_{\tilde{\chi}_1^\pm}$	545.2 GeV
Ωh^2	0.13	$m_{\tilde{\chi}_2^\pm}$	1136.2 GeV	Ωh^2	0.14	$m_{\tilde{\chi}_2^\pm}$	782.9 GeV
σ_p^{SI}	$6.78 \times 10^{-47} \text{cm}^2$	σ_p^{SD}	$4.54 \times 10^{-43} \text{cm}^2$	σ_p^{SI}	$4.64 \times 10^{-47} \text{cm}^2$	σ_p^{SD}	$4.16 \times 10^{-43} \text{cm}^2$
$N_{11}, N_{12}, N_{13}, N_{14}$	-0.997, 0.003, -0.071, 0.034			$N_{11}, N_{12}, N_{13}, N_{14}$	-0.998, 0.006, -0.066, 0.024		
$N_{21}, N_{22}, N_{23}, N_{24}$	0.074, 0.164, -0.698, 0.693			$N_{21}, N_{22}, N_{23}, N_{24}$	-0.023, -0.970, 0.197, -0.140		
$N_{31}, N_{32}, N_{33}, N_{34}$	0.027, -0.029, -0.706, -0.708			$N_{31}, N_{32}, N_{33}, N_{34}$	-0.030, 0.041, 0.705, 0.708		
$N_{41}, N_{42}, N_{43}, N_{44}$	-0.008, 0.986, 0.096, -0.136			$N_{41}, N_{42}, N_{43}, N_{44}$	-0.060, 0.239, 0.678, -0.692		
Annihilations	Fractions[%]			Annihilations	Fractions[%]		
$\bar{B} - \bar{\mu}_L$ Co-annihilation	92.6			$\bar{B} - \bar{\mu}_R$ Co-annihilation	95.2		
Decays	Branching ratios[%]			Decays	Branching ratios[%]		
$\tilde{\chi}_2^0 \rightarrow \tilde{\chi}_1^0 h/\tilde{\mu}_L^\pm \mu^\mp/\tilde{\chi}_1^0 Z/\tilde{\nu}_\mu \nu_\mu$	70.2/15.1/9.7/5.0			$\tilde{\chi}_2^0 \rightarrow \tilde{\chi}_1^0 h/\tilde{\chi}_1^0 Z/\tilde{\mu}_R^\pm \mu^\mp$	78.6/10.7/10.2		
$\tilde{\chi}_3^0 \rightarrow \tilde{\chi}_1^\pm Z/\tilde{\chi}_2^0 h/\tilde{\mu}_L^\pm \mu^\mp/\tilde{\nu}_\mu \nu_\mu$	86.7/10.8/1.6/0.8			$\tilde{\chi}_3^0 \rightarrow \tilde{\chi}_1^\pm W^\mp/\tilde{\chi}_2^0 Z/\tilde{\chi}_1^0 h/\tilde{\chi}_2^0 h/\tilde{\mu}_R^\pm \mu^\mp$	58.2/25.3/12.6/2.8/0.5/0.4		
$\tilde{\chi}_4^0 \rightarrow \tilde{\nu}_\mu \nu_\mu/\tilde{\mu}_L^\pm \mu^\mp/\tilde{\chi}_1^\pm W^\mp/\tilde{\chi}_2^0 Z/\tilde{\chi}_2^0 h/\tilde{\chi}_2^0 Z/\tilde{\chi}_1^0 h$	26.8/26.0/24.1/11.3/10.9/0.4/0.3			$\tilde{\chi}_4^0 \rightarrow \tilde{\chi}_1^\pm W^\mp/\tilde{\chi}_2^0 h/\tilde{\chi}_1^0 h/\tilde{\chi}_2^0 Z/\tilde{\nu}_\mu \nu_\mu/\tilde{\chi}_2^0 Z/\tilde{\mu}_L^\pm \mu^\mp/\tilde{\mu}_R^\pm \mu^\mp$	58.6/23.8/11.2/2.7/1.3/1.0/0.7/0.6		
$\tilde{\chi}_1^\pm \rightarrow \tilde{\chi}_1^0 W^\pm/\tilde{\nu}_\mu \mu^\pm/\tilde{\mu}_L^\pm \nu_\mu$	79.9/13.7/6.0			$\tilde{\chi}_1^\pm \rightarrow \tilde{\chi}_1^0 W^\pm/\tilde{\mu}_R^\pm \nu_\mu$	92.5/6.9		
$\tilde{\chi}_2^\pm \rightarrow \tilde{\mu}_L^\pm \nu_\mu/\tilde{\nu}_\mu \mu^\pm/\tilde{\chi}_1^\pm Z/\tilde{\chi}_3^0 W^\pm/\tilde{\chi}_1^\pm h$	26.3/26.1/12.8/11.9/11.7/11.2			$\tilde{\chi}_2^\pm \rightarrow \tilde{\chi}_2^0 W^\pm/\tilde{\chi}_1^\pm Z/\tilde{\chi}_1^\pm h/\tilde{\chi}_1^0 W^\pm/\tilde{\mu}_R^\pm \nu_\mu/\tilde{\nu}_\mu \mu^\pm$	31.4/28.4/24.6/13.3/1.3/0.8		
$\tilde{\mu}_L^\pm \rightarrow \tilde{\chi}_1^0 \mu^\pm$	100			$\tilde{\mu}_L^\pm \rightarrow \tilde{\chi}_1^0 \mu^\pm/\tilde{\chi}_1^\pm \nu_\mu/\tilde{\chi}_2^0 \mu^\pm/\tilde{\mu}_R^\pm h/\tilde{\mu}_R^\pm Z$	68.8/18.5/9.8/1.5/1.4		
$\tilde{\mu}_R^\pm \rightarrow \tilde{\chi}_1^0 \mu^\pm/\tilde{\chi}_2^0 \mu^\pm/\tilde{\nu}_\mu W^\pm/\tilde{\chi}_1^\pm \nu_\mu$	98.7/0.3/0.3/0.2			$\tilde{\mu}_R^\pm \rightarrow \tilde{\chi}_1^0 \mu^\pm$	100		
$\tilde{\nu}_\mu \rightarrow \tilde{\chi}_1^0 \nu_\mu$	100			$\tilde{\nu}_\mu \rightarrow \tilde{\chi}_1^0 \nu_\mu/\tilde{\chi}_1^\pm \mu^\mp/\tilde{\chi}_2^0 \nu_\mu/\tilde{\mu}_R^\pm W^\mp$	73.0/16.3/7.8/2.8		
R value	0.38, SR_A44 in SR-2			R value	0.50, SS15 in SR-2		

SRs that contributed to the largest R-values, and their capability to exclude the

Table 9. Benchmark points P5 for Type-E samples in Table 4 and P6 for the curved blue area on the $|m_{\tilde{\chi}_1^0} - m_{\tilde{\mu}_L}|$ plane in Fig. 5. P5 satisfies all the restrictions, while P6 is excluded by the LHC search for SUSY.

Benchmark Point P5 for Type-E samples				Benchmark Point P6 for the curved blue area in Fig. 5			
μ	719.2 GeV	m_H	3235.4 GeV	μ	551.2 GeV	m_H	6279.6 GeV
$\tan\beta$	38.7	m_A	3235.4 GeV	$\tan\beta$	31.7	m_A	6279.6 GeV
A_t	2697.6 GeV	m_h	125.7 GeV	A_t	2398.8 GeV	m_h	125.2 GeV
M_1	277.0 GeV	m_{H^\pm}	3253.2 GeV	M_1	-304.9 GeV	m_{H^\pm}	6284.5 GeV
M_2	1263.2 GeV	$m_{\tilde{\nu}_\mu}$	310.2 GeV	M_2	317.5 GeV	$m_{\tilde{\nu}_\mu}$	457.4 GeV
$\tilde{m}_{\tilde{\mu}_L}$	297.4 GeV	$m_{\tilde{\chi}_1^0}$	276.0 GeV	$\tilde{m}_{\tilde{\mu}_L}$	409.6 GeV	$m_{\tilde{\chi}_1^0}$	-304.1 GeV
$\tilde{m}_{\tilde{\mu}_R}$	288.2 GeV	$m_{\tilde{\chi}_2^0}$	731.5 GeV	$\tilde{m}_{\tilde{\mu}_R}$	755.9 GeV	$m_{\tilde{\chi}_2^0}$	327.2 GeV
$\tilde{m}_{\tilde{\mu}_L}$	321.0 GeV	$m_{\tilde{\chi}_3^0}$	-736.8 GeV	$\tilde{m}_{\tilde{\mu}_L}$	464.5 GeV	$m_{\tilde{\chi}_3^0}$	-570.1 GeV
$\tilde{m}_{\tilde{\mu}_R}$	279.6 GeV	$m_{\tilde{\chi}_4^0}$	1301.3 GeV	$\tilde{m}_{\tilde{\mu}_R}$	700.3 GeV	$m_{\tilde{\chi}_4^0}$	578.7 GeV
a_μ^{SUSY}	2.11×10^{-9}	$m_{\tilde{\chi}_1^\pm}$	730.8 GeV	a_μ^{SUSY}	2.03×10^{-9}	$m_{\tilde{\chi}_1^\pm}$	327.5 GeV
Ωh^2	0.13	$m_{\tilde{\chi}_2^\pm}$	1301.5 GeV	Ωh^2	0.10	$m_{\tilde{\chi}_2^\pm}$	581.0 GeV
σ_P^{SI}	$5.44 \times 10^{-47} \text{cm}^2$	σ_P^{SD}	$5.12 \times 10^{-43} \text{cm}^2$	σ_P^{SI}	$1.09 \times 10^{-46} \text{cm}^2$	σ_P^{SD}	$2.04 \times 10^{-42} \text{cm}^2$
$N_{11}, N_{12}, N_{13}, N_{14}$			-0.997, 0.002, -0.071, 0.028	$N_{11}, N_{12}, N_{13}, N_{14}$			-0.993, -0.007, -0.106, -0.055
$N_{21}, N_{22}, N_{23}, N_{24}$			0.070, 0.100, -0.703, 0.700	$N_{21}, N_{22}, N_{23}, N_{24}$			0.009, 0.971, -0.206, 0.122
$N_{31}, N_{32}, N_{33}, N_{34}$			0.030, -0.027, -0.706, -0.708	$N_{31}, N_{32}, N_{33}, N_{34}$			-0.114, 0.060, 0.697, 0.705
$N_{41}, N_{42}, N_{43}, N_{44}$			-0.004, 0.995, 0.052, -0.090	$N_{41}, N_{42}, N_{43}, N_{44}$			0.036, -0.232, -0.679, 0.696
Annihilations		Fractions[%]		Annihilations		Fractions[%]	
$\tilde{B} - \tilde{\mu}_R$ Co-annihilation		94.2		$\tilde{B} - \tilde{W}$ Co-annihilation		91.4	
Decays		Branching ratios[%]		Decays		Branching ratios[%]	
$\tilde{\chi}_2^0 \rightarrow \tilde{\chi}_1^0 h / \tilde{\chi}_1^0 Z / \tilde{\mu}_L^\pm \mu^\mp / \tilde{\mu}_R^\pm \mu^\mp / \tilde{\nu}_\mu \nu_\mu$		73.1/14.4/7.5/3.6/1.4		$\tilde{\chi}_2^0 \rightarrow \tilde{\chi}_1^0 Z^* / \tilde{\chi}_1^0 h^*$		100	
$\tilde{\chi}_3^0 \rightarrow \tilde{\chi}_1^0 Z / \tilde{\chi}_1^0 h / \tilde{\mu}_L^\pm \mu^\mp / \tilde{\mu}_R^\pm \mu^\mp / \tilde{\nu}_\mu \nu_\mu$		82.2/14.8/1.1/0.9/0.8		$\tilde{\chi}_3^0 \rightarrow \tilde{\chi}_1^\pm W^\mp / \tilde{\chi}_2^0 Z / \tilde{\chi}_1^0 h / \tilde{\chi}_2^0 h / \tilde{\chi}_1^0 Z$		62.1/27.0/8.1/1.4/1.1	
$\tilde{\chi}_4^0 \rightarrow \tilde{\chi}_1^\pm W^\mp / \tilde{\nu}_\mu \nu_\mu / \tilde{\mu}_L^\pm \mu^\mp / \tilde{\chi}_2^0 Z / \tilde{\chi}_3^0 Z / \tilde{\chi}_3^0 h / \tilde{\mu}_R^\pm \mu^\mp$		25.2/25.1/24.2/11.6/11.5/0.9/0.8/0.4		$\tilde{\chi}_4^0 \rightarrow \tilde{\chi}_1^\pm W^\mp / \tilde{\chi}_2^0 h / \tilde{\chi}_1^0 Z / \tilde{\chi}_2^0 Z / \tilde{\chi}_1^0 h / \tilde{\nu}_\mu \nu_\mu / \tilde{\mu}_L^\pm \mu^\mp$		63.6/24.0/8.2/2.2/0.8/0.7/0.5	
$\tilde{\chi}_1^\pm \rightarrow \tilde{\chi}_2^\pm W^\pm / \tilde{\nu}_\mu \nu_\mu / \tilde{\mu}_L^\pm \mu^\pm / \tilde{\mu}_R^\pm \mu^\pm$		89.7/7.0/1.7/1.1		$\tilde{\chi}_1^\pm \rightarrow \tilde{\chi}_1^0 (W^\pm)^*$		100	
$\tilde{\chi}_2^\pm \rightarrow \tilde{\nu}_\mu \mu^\pm / \tilde{\mu}_L^\pm \nu_\mu / \tilde{\chi}_3^\pm Z / \tilde{\chi}_3^\pm h / \tilde{\chi}_3^\pm W^\pm / \tilde{\chi}_1^\pm h$		24.8/24.4/12.8/12.5/12.5/12.4		$\tilde{\chi}_2^\pm \rightarrow \tilde{\chi}_2^0 W^\pm / \tilde{\chi}_1^\pm Z / \tilde{\chi}_1^\pm h / \tilde{\chi}_1^\pm W^\pm / \tilde{\mu}_L^\pm \nu_\mu / \tilde{\nu}_\mu \mu^\pm$		32.3/30.4/25.7/10.3/0.9/0.4	
$\tilde{\mu}_L^\pm \rightarrow \tilde{\chi}_1^0 \mu^\pm$		100		$\tilde{\mu}_L^\pm \rightarrow \tilde{\chi}_1^\pm \nu_\mu / \tilde{\chi}_3^0 \mu^\pm / \tilde{\chi}_1^0 \mu^\pm$		57.2/29.8/13.0	
$\tilde{\mu}_R^\pm \rightarrow \tilde{\chi}_1^0 \mu^\pm$		100		$\tilde{\mu}_R^\pm \rightarrow \tilde{\chi}_1^0 \mu^\pm / \tilde{\chi}_3^0 \mu^\pm$		99.5/0.2	
$\tilde{\nu}_\mu \rightarrow \tilde{\chi}_1^0 \nu_\mu$		100		$\tilde{\nu}_\mu \rightarrow \tilde{\chi}_1^\pm \mu^\mp / \tilde{\chi}_3^0 \nu_\mu / \tilde{\chi}_1^0 \nu_\mu$		59.2/28.5/12.3	
R value		0.34, SR_A44 in SR-2		R value		1.22, SR_WZoff_high_njd in SR-4	

Table 10. Survival mechanisms for the six benchmark points listed in Tables 7–9. These mechanisms rely on both the properties of the points and experimental search strategies. They are acquired by comparing the dominant signals of the productions with relevant experimental data.

Survival mechanism \ Points	P1	P2	P3	P4	P5	P6
Production						
$\tilde{W}\tilde{W}$	I, II [112]	I, II [124]	III, IV [113]	I, IV [113]	IV [113]	I, II [112]
$\tilde{H}\tilde{H}$	I, III, IV [112]	III, IV [124]	IV [113]	III, IV [113]	IV [113]	III [112]
$\tilde{\mu}_L^* \tilde{\mu}_L$	I, III, IV [6]	I, II [124]	I, II [124]	IV [6]	I, II [124]	III [6]
$\tilde{\mu}_R^* \tilde{\mu}_R$	I, IV [6]	IV [6]	IV [6]	I, II [124]	I, II [124]	IV [6]

samples of each mechanism, expressed by the percentage of the total numbers in the second column. The following SRs are involved:

- SR-1: Signal regions **SRG08_0j_mll** and **SRG07_0j_mll** defined in Ref. [6]. These come from the LHC search for slepton pair production by the final state containing two opposite-sign-same-flavor (OSSF) leptons and missing transverse momentum.
- SR-2: Signal regions **SR_A44**, **SS15**, and **SR_A08** in Ref. [113, 114]. They arise from the LHC search for electroweakinos with the final state containing missing transverse momentum, no jets, and two same-sign (SS) dileptons for the SS15, three electrons, or muons that form at least one OSSF pair for the SR_A44 and SR_A08.

- SR-3: Signal regions **E - high - mm - 30**, **S - high - mm - 05**, **S - high - mm - 10**, and so on proposed in Ref. [124]. Their study concentrated on the electroweakinos with compressed mass spectra and investigated their production at the LHC by the final state containing two leptons and missing transverse momentum.
- SR-4: Signal regions **SR_incWZoff_high_njc1**, **SR_WZoff_high_njd**, **SR_WZoff_high_njc**, and so on defined in Ref. [112]. These authors studied the chargino–neutralino associated production at the LHC by the final state containing three leptons and missing transverse momentum, where the chargino and neutralino decayed into off-shell W and Z bosons, respectively.
- SR-5: Signal regions **SR1_weakino_3high_mll_2**, **SR2_stop_3high_pt_1**, and **SR1_weakino_2media_mll_2** defined in Ref. [126]. These arise from the LHC search for new physics by the signal containing two soft oppositely charged leptons and missing transverse momentum.

These revealed how these annihilation mechanisms have been tested at the LHC. In particular, Table 6 shows that different SRs complement each other in doing so, and a single SR never plays a dominant role in this regard. This conclusion depends not only on the intrinsic physics of the MSSM but also on the details of these SRs. It arises from the fact that we include as many experimental analyses as possible to study the LHC restrictions, and each of them usually defines several signal regions. This situation allows us to make good use of the experimental data to explore the parameter space of the MSSM.

Next, we illuminate how the MSSM manages to survive the LHC restriction. We looked for benchmark points from the Type-A, B, C, D, and E samples specified in Table 4 and labeled them P1, P2, P3, P4, and P5, respectively. We present their details in Tables 7, 8, and 9, and provide corresponding survival mechanisms in Table 10. These mechanisms are acquired by comparing the dominant signals of the productions with pertinent experimental data. For example, the DM in P1 achieved the measured density by co-annihilating with wino-like particles. The applicable restriction to the wino productions came from the search for the chargino–neutralino associated production, where the chargino and neutralino decayed into off-shell W and Z bosons, respectively. The most robust results came from the analysis in Ref. [112], and they served as the guidelines of our judgment. We also provided a benchmark point, P6, for the curved blue area on the $|m_{\tilde{\chi}_1^0}| - m_{\tilde{\mu}_L}$ plane in Fig. 5, characterized by $230 \text{ GeV} \lesssim |m_{\tilde{\chi}_1^0}| \lesssim 350 \text{ GeV}$ and $300 \text{ GeV} \lesssim m_{\tilde{\mu}_L} \lesssim 500 \text{ GeV}$. Our simulation indicated that it is excluded by **SR_WZoff_high_njd** in SR-4, which is designed for the tri-lepton signal from off-shell W and Z bosons. This point is distinct because both the wino pair production and the $\tilde{\mu}_L$ pair production contribute to this signal,

and none of these processes alone can exclude this point. In addition, the program `SModelS-2.2.1` is also unable to exclude it since it misses the $\tilde{\mu}_L$ contribution.

At this stage, we clarify the following points about the LHC restrictions:

- Throughout this study, both the theoretical uncertainties incurred in the simulations and the experimental (systematic and statistic) uncertainties were not included. Although these effects can relax the LHC restrictions, it is expected that much stronger restrictions on the MSSM will be acquired given the advent of high-luminosity LHC in the near future.
- We did not include the search for charginos and neutralinos by the fully hadronic final states of W/Z and Higgs bosons with 139 fb^{-1} data [170] in this study. This search rejects large SM backgrounds by identifying high- p_T bosons with large-radius jets and jet substructure information. Thus, it is more efficient than the leptonic signal search in Ref. [112] only when winos are heavier than 600 GeV [170]. This conclusion holds in simplified models of SUSY but was never applied to this research. The reason is that the DM must co-annihilate with $\tilde{\mu}_L$ or $\tilde{\mu}_R$ to achieve the measured density for $M_2 \gtrsim 600 \text{ GeV}$ (see the results in Fig. 2), and the wino-like particles may decay into the slepton first to enhance their leptonic signal. As a result, it is the leptonic signals that are more powerful in excluding SUSY points. This conclusion is the same as that of the General Next-to-Minimal Supersymmetric Standard Model (GNMSSM) studied in Ref. [89].

In the latest version of SModelS, namely SModelS-2.2.1 [165], the cut efficiencies of the hadronic analysis and relevant signal topologies have been implemented in its database. We utilized this code to limit the green samples in Fig. 1. We did not find that it has exclusion capabilities.

- In some high-energy SUSY-breaking theories, $\tilde{\tau}$ may be the NLSP due to its larger Yukawa coupling than those of the first- and second-generation sleptons. In this case, heavy sparticles may decay into $\tilde{\tau}$ to change the e/μ signals of this research, and the LHC restrictions may be relaxed [46]. We will discuss such a possibility in our future work.

3.4 Related issues

We stress the following issues related to this research:

- Throughout this study, we assumed that $\tilde{\chi}_1^0$ was fully responsible for the measured density. This assumption determined that the DM is bino-dominated and approximately degenerate with winos or sleptons in mass. This has profound implications on the phenomenology of the MSSM. Relaxing this assumption usually complicates this kind of research and makes the obtained conclusions untenable [98].

- As pointed out by the recent lattice simulation of the BMW collaboration on the hadronic vacuum polarization contribution to a_μ [31], the muon g-2 anomaly may arise from the uncertainties in calculating the hadronic contribution to the moment. If this speculation is corroborated, a_μ^{SUSY} should be much smaller than its currently favored size, and any of the electroweakinos and $\tilde{\mu}_{L/R}$ are not necessarily light. In this case, the LHC restrictions will be relaxed significantly. For example, we recently updated the results of Ref. [171], which only studied the DM physics in GNMSSM, by including the recent LZ restrictions. We found that the analyses in Table 1 only excluded about 4% of the remaining samples in Fig. 2 of Ref. [171].
- It is remarkable that the explanations of the anomaly in the MSSM are to be tested at future colliders, given that it predicts some moderately light sparticles, such as $m_{\tilde{\chi}_1^0}$, m_{NLSP} , and m_{NNLSP} . It was found that although only parts of the preferred parameter space can be covered in the high-luminosity LHC, exhaustive coverage of the parameter space is possible at a high-energy e^+e^- collider with $\sqrt{s} \gtrsim 1$ TeV, such as ILC with $\sqrt{s} = 1$ TeV [172] and CLIC with $\sqrt{s} = 1$ TeV [173, 174]. This conclusion was acquired from Fig. 4 of Ref. [175], where the capabilities of different colliders to survey the explanation were compared for the $\tilde{B} - \tilde{W}$ co-annihilation case.

4 Summary

Inspired by the rapid progress of particle physics experiments in recent years, we studied their impacts on the MSSM and how the theory kept consistent with them. We are particularly interested in the recent measurement of the muon g-2 at Fermilab, the LHC search for SUSY, and the DM direct detection by the LZ experiment since they are sensitive to different parameters and complement each other to provide valuable information of the MSSM. In surveying the status of the MSSM, we utilized the MultiNest algorithm to comprehensively scan its parameter space. We adopted the muon g-2 observable to guide the scans and include the restrictions from the LHC Higgs data, DM experiments, B-physics measurements, and vacuum stability. We also examined the samples acquired from the scans by the restrictions from the LHC search for SUSY and the latest LZ experiment. The main conclusions of this research are as follows:

- The bino-dominated DM achieved the measured relic density by co-annihilating with wino-like electroweakinos, $\tilde{\mu}_L$, or $\tilde{\mu}_R$ if one intends the theory to explain the muon g-2 anomaly.
- Given the measured DM density, the LZ experiment alone has required $\mu \gtrsim 380$ GeV for $M_1 < 0$ and $\mu \gtrsim 600$ GeV for $M_1 > 100$ GeV. If the restrictions

from the muon $g-2$ anomaly and the LHC experiment are also included, the lower bounds become about 500 GeV and 630 GeV, respectively, indicating that the theory needs a tuning of $\mathcal{O}(1\%)$ to predict Z -boson mass [168]. Compared with the restriction from the PandaX-4T experiment on the SI scattering cross section, these bounds are improved by about 100 GeV. This situation makes the Z - and h -mediated resonant annihilations even more unnatural so that they are usually missed in the scans by the MultiNest algorithm. The fundamental reason of such phenomena is the correlation between the DM physics and the electroweak symmetry breaking in the MSSM.

- Based on the premise of explaining the muon $g-2$ anomaly at the 2σ level, the LHC restrictions have set bounds on the sparticle mass spectra: $m_{\tilde{\chi}_1^0} \gtrsim 210$ GeV, $m_{\tilde{\chi}_2^0}, m_{\tilde{\chi}_1^\pm} \gtrsim 235$ GeV, $m_{\tilde{\chi}_3^0} \gtrsim 515$ GeV, $m_{\tilde{\chi}_4^0} \gtrsim 525$ GeV, $m_{\tilde{\chi}_2^\pm} \gtrsim 530$ GeV, $m_{\tilde{\nu}_\mu} \gtrsim 235$ GeV, $m_{\tilde{\mu}_1} \gtrsim 215$ GeV, and $m_{\tilde{\mu}_2} \gtrsim 250$ GeV, where $\tilde{\chi}_2^0$ and $\tilde{\chi}_1^\pm$ are wino-dominated when they are lighter than about 500 GeV and $m_{\tilde{\mu}_1}$ may be either $m_{\tilde{\mu}_L}$ or $m_{\tilde{\mu}_R}$. These bounds should be regarded as rough estimates, instead of accurate values, since the samples studied in this research are far from sufficient given the broad parameter space of the MSSM. In addition, these bounds are far beyond the reach of the LEP experiments in searching for SUSY and have not been acquired before.

The results can be interpreted as follows: if $\tilde{\chi}_1^0$ is lighter, more missing transverse energy will be emitted in the sparticle production processes at the LHC, which can improve the sensitivities of the experimental analyses. However, the sparticles other than $\tilde{\chi}_1^0$ are lighter, and they will be more copiously produced at the LHC to increase the events containing multiple leptons.

- We illuminate how some parameter spaces of the MSSM have been tested at the LHC in Table 6. We also list five scenarios that are consistent with the LHC restrictions in Table 4 and explain why they can do so by presenting benchmark points in Tables 7–9, and their survival mechanisms are shown in Table 10.

This work extends the previous studies of the muon $g-2$ anomaly in the MSSM, in particular those of Refs. [84] and [85], by utilizing more sophisticated research strategies and surveying the LHC restrictions comprehensively. As a result, the conclusions acquired in this research are more robust than those in previous works. They exhibit the most essential characteristics of the MSSM.

5 Acknowledgement

We sincerely thank Prof. Junjie Cao for numerous helpful discussions and his great efforts to improve the manuscript. This work is supported by the National Natural

Science Foundation of China (NNSFC) under grant Nos. 12075076 and 11905044.

References

- [1] P. Fayet and S. Ferrara, *Supersymmetry*, *Phys. Rept.* **32** (1977) 249.
- [2] H. E. Haber and G. L. Kane, *The Search for Supersymmetry: Probing Physics Beyond the Standard Model*, *Phys. Rept.* **117** (1985) 75.
- [3] S. P. Martin, *A Supersymmetry primer*, [hep-ph/9709356](#).
- [4] G. Jungman, M. Kamionkowski and K. Griest, *Supersymmetric dark matter*, *Phys. Rept.* **267** (1996) 195 [[hep-ph/9506380](#)].
- [5] ATLAS collaboration, G. Aad et al., *Search for electroweak production of charginos and sleptons decaying into final states with two leptons and missing transverse momentum in $\sqrt{s} = 13$ TeV pp collisions using the ATLAS detector*, *Eur. Phys. J. C* **80** (2020) 123 [[1908.08215](#)].
- [6] CMS collaboration, A. M. Sirunyan et al., *Search for supersymmetry in final states with two oppositely charged same-flavor leptons and missing transverse momentum in proton-proton collisions at $\sqrt{s} = 13$ TeV*, *JHEP* **04** (2021) 123 [[2012.08600](#)].
- [7] LZ collaboration, J. Aalbers et al., *First Dark Matter Search Results from the LUX-ZEPLIN (LZ) Experiment*, [2207.03764](#).
- [8] MUON G-2 collaboration, G. W. Bennett et al., *Final Report of the Muon E821 Anomalous Magnetic Moment Measurement at BNL*, *Phys. Rev. D* **73** (2006) 072003 [[hep-ex/0602035](#)].
- [9] MUON G-2 collaboration, B. Abi et al., *Measurement of the Positive Muon Anomalous Magnetic Moment to 0.46 ppm*, *Phys. Rev. Lett.* **126** (2021) 141801 [[2104.03281](#)].
- [10] T. Aoyama et al., *The anomalous magnetic moment of the muon in the Standard Model*, *Phys. Rept.* **887** (2020) 1 [[2006.04822](#)].
- [11] T. Aoyama, M. Hayakawa, T. Kinoshita and M. Nio, *Complete Tenth-Order QED Contribution to the Muon $g - 2$* , *Phys. Rev. Lett.* **109** (2012) 111808 [[1205.5370](#)].
- [12] T. Aoyama, T. Kinoshita and M. Nio, *Theory of the Anomalous Magnetic Moment of the Electron*, *Atoms* **7** (2019) 28.
- [13] A. Czarnecki, W. J. Marciano and A. Vainshtein, *Refinements in electroweak contributions to the muon anomalous magnetic moment*, *Phys. Rev.* **D67** (2003) 073006 [[hep-ph/0212229](#)].
- [14] C. Gnendiger, D. Stöckinger and H. Stöckinger-Kim, *The electroweak contributions to $(g - 2)_\mu$ after the Higgs boson mass measurement*, *Phys. Rev.* **D88** (2013) 053005 [[1306.5546](#)].
- [15] M. Davier, A. Hoecker, B. Malaescu and Z. Zhang, *Reevaluation of the hadronic vacuum polarisation contributions to the Standard Model predictions of the muon*

- $g - 2$ and $\alpha(m_Z^2)$ using newest hadronic cross-section data, *Eur. Phys. J. C* **77** (2017) 827 [[1706.09436](#)].
- [16] A. Keshavarzi, D. Nomura and T. Teubner, *Muon $g - 2$ and $\alpha(M_Z^2)$: a new data-based analysis*, *Phys. Rev. D* **97** (2018) 114025 [[1802.02995](#)].
 - [17] G. Colangelo, M. Hoferichter and P. Stoffer, *Two-pion contribution to hadronic vacuum polarization*, *JHEP* **02** (2019) 006 [[1810.00007](#)].
 - [18] M. Hoferichter, B.-L. Hoid and B. Kubis, *Three-pion contribution to hadronic vacuum polarization*, *JHEP* **08** (2019) 137 [[1907.01556](#)].
 - [19] M. Davier, A. Hoecker, B. Malaescu and Z. Zhang, *A new evaluation of the hadronic vacuum polarisation contributions to the muon anomalous magnetic moment and to $\alpha(m_Z^2)$* , *Eur. Phys. J. C* **80** (2020) 241 [[1908.00921](#)].
 - [20] A. Keshavarzi, D. Nomura and T. Teubner, *The $g - 2$ of charged leptons, $\alpha(M_Z^2)$ and the hyperfine splitting of muonium*, *Phys. Rev. D* **101** (2020) 014029 [[1911.00367](#)].
 - [21] A. Kurz, T. Liu, P. Marquard and M. Steinhauser, *Hadronic contribution to the muon anomalous magnetic moment to next-to-next-to-leading order*, *Phys. Lett. B* **734** (2014) 144 [[1403.6400](#)].
 - [22] K. Melnikov and A. Vainshtein, *Hadronic light-by-light scattering contribution to the muon anomalous magnetic moment revisited*, *Phys. Rev. D* **70** (2004) 113006 [[hep-ph/0312226](#)].
 - [23] P. Masjuan and P. Sánchez-Puertas, *Pseudoscalar-pole contribution to the $(g_\mu - 2)$: a rational approach*, *Phys. Rev. D* **95** (2017) 054026 [[1701.05829](#)].
 - [24] G. Colangelo, M. Hoferichter, M. Procura and P. Stoffer, *Dispersion relation for hadronic light-by-light scattering: two-pion contributions*, *JHEP* **04** (2017) 161 [[1702.07347](#)].
 - [25] M. Hoferichter, B.-L. Hoid, B. Kubis, S. Leupold and S. P. Schneider, *Dispersion relation for hadronic light-by-light scattering: pion pole*, *JHEP* **10** (2018) 141 [[1808.04823](#)].
 - [26] A. Gérardin, H. B. Meyer and A. Nyffeler, *Lattice calculation of the pion transition form factor with $N_f = 2 + 1$ Wilson quarks*, *Phys. Rev. D* **100** (2019) 034520 [[1903.09471](#)].
 - [27] J. Bijnens, N. Hermansson-Truedsson and A. Rodríguez-Sánchez, *Short-distance constraints for the $HLbL$ contribution to the muon anomalous magnetic moment*, *Phys. Lett. B* **798** (2019) 134994 [[1908.03331](#)].
 - [28] G. Colangelo, F. Hagelstein, M. Hoferichter, L. Laub and P. Stoffer, *Longitudinal short-distance constraints for the hadronic light-by-light contribution to $(g - 2)_\mu$ with large- N_c Regge models*, *JHEP* **03** (2020) 101 [[1910.13432](#)].
 - [29] T. Blum, N. Christ, M. Hayakawa, T. Izubuchi, L. Jin, C. Jung et al., *The hadronic*

- light-by-light scattering contribution to the muon anomalous magnetic moment from lattice QCD, *Phys. Rev. Lett.* **124** (2020) 132002 [[1911.08123](#)].
- [30] G. Colangelo, M. Hoferichter, A. Nyffeler, M. Passera and P. Stoffer, *Remarks on higher-order hadronic corrections to the muon $g - 2$* , *Phys. Lett.* **B735** (2014) 90 [[1403.7512](#)].
 - [31] S. Borsanyi et al., *Leading hadronic contribution to the muon magnetic moment from lattice QCD*, *Nature* **593** (2021) 51 [[2002.12347](#)].
 - [32] P. Athron, C. Balázs, D. H. Jacob, W. Kotlarski, D. Stöckinger and H. Stöckinger-Kim, *New physics explanations of a_μ in light of the FNAL muon $g - 2$ measurement*, [2104.03691](#).
 - [33] S. P. Martin and J. D. Wells, *Muon Anomalous Magnetic Dipole Moment in Supersymmetric Theories*, *Phys. Rev. D* **64** (2001) 035003 [[hep-ph/0103067](#)].
 - [34] F. Domingo and U. Ellwanger, *Constraints from the Muon $g-2$ on the Parameter Space of the NMSSM*, *JHEP* **07** (2008) 079 [[0806.0733](#)].
 - [35] T. Moroi, *The Muon anomalous magnetic dipole moment in the minimal supersymmetric standard model*, *Phys. Rev. D* **53** (1996) 6565 [[hep-ph/9512396](#)].
 - [36] W. Hollik, J. I. Illana, S. Rigolin and D. Stockinger, *One loop MSSM contribution to the weak magnetic dipole moments of heavy fermions*, *Phys. Lett. B* **416** (1998) 345 [[hep-ph/9707437](#)].
 - [37] P. Athron, M. Bach, H. G. Fargnoli, C. Gnendiger, R. Greifenhagen, J.-h. Park et al., *GM2Calc: Precise MSSM prediction for $(g - 2)$ of the muon*, *Eur. Phys. J. C* **76** (2016) 62 [[1510.08071](#)].
 - [38] M. Endo, K. Hamaguchi, S. Iwamoto and T. Kitahara, *Supersymmetric interpretation of the muon $g - 2$ anomaly*, *JHEP* **07** (2021) 075 [[2104.03217](#)].
 - [39] D. Stockinger, *The Muon Magnetic Moment and Supersymmetry*, *J. Phys. G* **34** (2007) R45 [[hep-ph/0609168](#)].
 - [40] A. Czarnecki and W. J. Marciano, *The Muon anomalous magnetic moment: A Harbinger for 'new physics'*, *Phys. Rev. D* **64** (2001) 013014 [[hep-ph/0102122](#)].
 - [41] J. Cao, Z. Heng, D. Li and J. M. Yang, *Current experimental constraints on the lightest Higgs boson mass in the constrained MSSM*, *Phys. Lett. B* **710** (2012) 665 [[1112.4391](#)].
 - [42] M. Endo, K. Hamaguchi, T. Kitahara and T. Yoshinaga, *Probing Bino contribution to muon $g - 2$* , *JHEP* **11** (2013) 013 [[1309.3065](#)].
 - [43] Z. Kang, *$H_{u,d}$ -messenger Couplings Address the $\mu/B_\mu \setminus \mathcal{E} A_t/m_{H_u}^2$ Problem and $(g - 2)_\mu$ Puzzle*, [1610.06024](#).
 - [44] B. Zhu, R. Ding and T. Li, *Higgs mass and muon anomalous magnetic moment in the MSSM with gauge-gravity hybrid mediation*, *Phys. Rev. D* **96** (2017) 035029 [[1610.09840](#)].

- [45] T. T. Yanagida and N. Yokozaki, *Muon $g - 2$ in MSSM gauge mediation revisited*, *Phys. Lett. B* **772** (2017) 409 [[1704.00711](#)].
- [46] K. Hagiwara, K. Ma and S. Mukhopadhyay, *Closing in on the chargino contribution to the muon $g-2$ in the MSSM: current LHC constraints*, *Phys. Rev. D* **97** (2018) 055035 [[1706.09313](#)].
- [47] P. Cox, C. Han and T. T. Yanagida, *Muon $g - 2$ and dark matter in the minimal supersymmetric standard model*, *Phys. Rev. D* **98** (2018) 055015 [[1805.02802](#)].
- [48] H. M. Tran and H. T. Nguyen, *GUT-inspired MSSM in light of muon $g - 2$ and LHC results at $\sqrt{s} = 13$ TeV*, *Phys. Rev. D* **99** (2019) 035040 [[1812.11757](#)].
- [49] B. P. Padley, K. Sinha and K. Wang, *Natural Supersymmetry, Muon $g - 2$, and the Last Crevices for the Top Squark*, *Phys. Rev. D* **92** (2015) 055025 [[1505.05877](#)].
- [50] A. Choudhury, L. Darmé, L. Roszkowski, E. M. Sessolo and S. Trojanowski, *Muon $g - 2$ and related phenomenology in constrained vector-like extensions of the MSSM*, *JHEP* **05** (2017) 072 [[1701.08778](#)].
- [51] N. Okada and H. M. Tran, *125 GeV Higgs boson mass and muon $g - 2$ in 5D MSSM*, *Phys. Rev. D* **94** (2016) 075016 [[1606.05329](#)].
- [52] X. Du and F. Wang, *NMSSM From Alternative Deflection in Generalized Deflected Anomaly Mediated SUSY Breaking*, *Eur. Phys. J. C* **78** (2018) 431 [[1710.06105](#)].
- [53] X. Ning and F. Wang, *Solving the muon $g-2$ anomaly within the NMSSM from generalized deflected AMSB*, *JHEP* **08** (2017) 089 [[1704.05079](#)].
- [54] K. Wang, F. Wang, J. Zhu and Q. Jie, *The semi-constrained NMSSM in light of muon $g-2$, LHC, and dark matter constraints*, *Chin. Phys. C* **42** (2018) 103109 [[1811.04435](#)].
- [55] J.-L. Yang, T.-F. Feng, Y.-L. Yan, W. Li, S.-M. Zhao and H.-B. Zhang, *Lepton-flavor violation and two loop electroweak corrections to $(g - 2)_\mu$ in the B-L symmetric SSM*, *Phys. Rev. D* **99** (2019) 015002 [[1812.03860](#)].
- [56] C.-X. Liu, H.-B. Zhang, J.-L. Yang, S.-M. Zhao, Y.-B. Liu and T.-F. Feng, *Higgs boson decay $h \rightarrow Z\gamma$ and muon magnetic dipole moment in the $\mu\nu$ SSM*, *JHEP* **04** (2020) 002 [[2002.04370](#)].
- [57] J. Cao, J. Lian, L. Meng, Y. Yue and P. Zhu, *Anomalous muon magnetic moment in the inverse seesaw extended next-to-minimal supersymmetric standard model*, *Phys. Rev. D* **101** (2020) 095009 [[1912.10225](#)].
- [58] J. Cao, Y. He, J. Lian, D. Zhang and P. Zhu, *Electron and muon anomalous magnetic moments in the inverse seesaw extended NMSSM*, *Phys. Rev. D* **104** (2021) 055009 [[2102.11355](#)].
- [59] W. Ke and P. Slavich, *Higgs-mass constraints on a supersymmetric solution of the muon $g-2$ anomaly*, [2109.15277](#).

- [60] J. L. Lamborn, T. Li, J. A. Maxin and D. V. Nanopoulos, *Resolving the $(g - 2)_\mu$ Discrepancy with \mathcal{F} -SU(5) Intersecting D-branes*, [2108.08084](#).
- [61] S. Li, Y. Xiao and J. M. Yang, *Constraining CP-phases in SUSY: an interplay of muon/electron $g - 2$ and electron EDM*, [2108.00359](#).
- [62] Y. Nakai, M. Reece and M. Suzuki, *Supersymmetric alignment models for $(g-2)_\mu$* , *JHEP* **10** (2021) 068 [[2107.10268](#)].
- [63] S. Li, Y. Xiao and J. M. Yang, *Can electron and muon $g - 2$ anomalies be jointly explained in SUSY?*, [2107.04962](#).
- [64] J. S. Kim, D. E. Lopez-Fogliani, A. D. Perez and R. R. de Austri, *The new $(g - 2)_\mu$ and Right-Handed Sneutrino Dark Matter*, [2107.02285](#).
- [65] Z. Li, G.-L. Liu, F. Wang, J. M. Yang and Y. Zhang, *Gluino-SUGRA scenarios in light of FNAL muon $g-2$ anomaly*, [2106.04466](#).
- [66] W. Altmannshofer, S. A. Gadam, S. Gori and N. Hamer, *Explaining $(g - 2)_\mu$ with Multi-TeV Sleptons*, [2104.08293](#).
- [67] H. Baer, V. Barger and H. Serce, *Anomalous muon magnetic moment, supersymmetry, naturalness, LHC search limits and the landscape*, *Phys. Lett. B* **820** (2021) 136480 [[2104.07597](#)].
- [68] M. Chakraborti, L. Roszkowski and S. Trojanowski, *GUT-constrained supersymmetry and dark matter in light of the new $(g - 2)_\mu$ determination*, *JHEP* **05** (2021) 252 [[2104.04458](#)].
- [69] A. Aboubrahim, M. Klasen and P. Nath, *What the Fermilab muon $g-2$ experiment tells us about discovering supersymmetry at high luminosity and high energy upgrades to the LHC*, *Phys. Rev. D* **104** (2021) 035039 [[2104.03839](#)].
- [70] S. Iwamoto, T. T. Yanagida and N. Yokozaki, *Wino-Higgsino dark matter in MSSM from the $g-2$ anomaly*, *Phys. Lett. B* **823** (2021) 136768 [[2104.03223](#)].
- [71] M. Chakraborti, S. Heinemeyer and I. Saha, *The new “MUON $G-2$ ” result and supersymmetry*, *Eur. Phys. J. C* **81** (2021) 1114 [[2104.03287](#)].
- [72] J. Cao, J. Lian, Y. Pan, D. Zhang and P. Zhu, *Improved $(g - 2)_\mu$ measurement and singlino dark matter in μ -term extended \mathbb{Z}_3 -NMSSM*, *JHEP* **09** (2021) 175 [[2104.03284](#)].
- [73] W. Yin, *Muon $g - 2$ anomaly in anomaly mediation*, *JHEP* **06** (2021) 029 [[2104.03259](#)].
- [74] H.-B. Zhang, C.-X. Liu, J.-L. Yang and T.-F. Feng, *Muon anomalous magnetic dipole moment in the $\mu\nu$ SSM*, [2104.03489](#).
- [75] M. Ibe, S. Kobayashi, Y. Nakayama and S. Shirai, *Muon $g - 2$ in Gauge Mediation without SUSY CP Problem*, [2104.03289](#).
- [76] M.-D. Zheng and H.-H. Zhang, *Studying the $b \rightarrow s\ell^+\ell^-$ anomalies and $(g - 2)_\mu$ in*

- R-parity violating MSSM framework with the inverse seesaw mechanism*, *Phys. Rev. D* **104** (2021) 115023 [[2105.06954](#)].
- [77] C. Han, *Muon $g-2$ and CP violation in MSSM*, [2104.03292](#).
 - [78] F. Wang, L. Wu, Y. Xiao, J. M. Yang and Y. Zhang, *GUT-scale constrained SUSY in light of new muon $g-2$ measurement*, *Nucl. Phys. B* **970** (2021) 115486 [[2104.03262](#)].
 - [79] M.-D. Zheng and H.-H. Zhang, *Studying the $b \rightarrow s\ell + \ell^-$ anomalies and $(g-2)_\mu$ in R-parity violating MSSM framework with the inverse seesaw mechanism*, *Phys. Rev. D* **104** (2021) 115023.
 - [80] M. Chakraborti, S. Heinemeyer, I. Saha and C. Schappacher, *$(g-2)_\mu$ and SUSY Dark Matter: Direct Detection and Collider Search Complementarity*, [2112.01389](#).
 - [81] A. Aboubrahim, M. Klasen, P. Nath and R. M. Syed, *Tests of gluino-driven radiative breaking of the electroweak symmetry at the LHC*, in *10th International Conference on New Frontiers in Physics*, 12, 2021, [2112.04986](#).
 - [82] M. I. Ali, M. Chakraborti, U. Chattopadhyay and S. Mukherjee, *Muon and Electron $(g-2)$ Anomalies with Non-Holomorphic Interactions in MSSM*, [2112.09867](#).
 - [83] K. Wang and J. Zhu, *A smuon in the NMSSM confronted with the muon $g-2$ and SUSY searches*, [2112.14576](#).
 - [84] M. Chakraborti, S. Heinemeyer and I. Saha, *Improved $(g-2)_\mu$ Measurements and Supersymmetry*, *Eur. Phys. J. C* **80** (2020) 984 [[2006.15157](#)].
 - [85] S. Baum, M. Carena, N. R. Shah and C. E. M. Wagner, *The tiny $(g-2)$ muon wobble from small- μ supersymmetry*, *JHEP* **01** (2022) 025 [[2104.03302](#)].
 - [86] J. Cao, J. Lian, Y. Pan, Y. Yue and D. Zhang, *Impact of recent $(g-2)_\mu$ measurement on the light CP-even Higgs scenario in general Next-to-Minimal Supersymmetric Standard Model*, *JHEP* **03** (2022) 203 [[2201.11490](#)].
 - [87] J. Cao, F. Li, J. Lian, Y. Pan and D. Zhang, *Impact of LHC probes of SUSY and recent measurement of $(g-2)_\mu$ on \mathbb{Z}_3 -NMSSM*, *Sci. China Phys. Mech. Astron.* **65** (2022) 291012 [[2204.04710](#)].
 - [88] F. Domingo, U. Ellwanger and C. Hugonie, *M_W , Dark Matter and a_μ in the NMSSM*, [2209.03863](#).
 - [89] J. Cao, X. Jia, L. Meng, Y. Yue and D. Zhang, *Status of the singlino-dominated dark matter in general Next-to-Minimal Supersymmetric Standard Model*, [2210.08769](#).
 - [90] J. F. Gunion and H. E. Haber, *Higgs Bosons in Supersymmetric Models. 1.*, *Nucl. Phys. B* **272** (1986) 1.
 - [91] A. Djouadi, *The Anatomy of electro-weak symmetry breaking. II. The Higgs bosons in the minimal supersymmetric model*, *Phys. Rept.* **459** (2008) 1 [[hep-ph/0503173](#)].

- [92] ATLAS collaboration, G. Aad et al., *Search for heavy Higgs bosons decaying into two tau leptons with the ATLAS detector using pp collisions at $\sqrt{s} = 13$ TeV*, *Phys. Rev. Lett.* **125** (2020) 051801 [[2002.12223](#)].
- [93] ATLAS collaboration, G. Aad et al., *Search for charged Higgs bosons decaying into a top quark and a bottom quark at $\sqrt{s} = 13$ TeV with the ATLAS detector*, *JHEP* **06** (2021) 145 [[2102.10076](#)].
- [94] S. Dimopoulos and D. W. Sutter, *The Supersymmetric flavor problem*, *Nucl. Phys. B* **452** (1995) 496 [[hep-ph/9504415](#)].
- [95] F. Gabbiani, E. Gabrielli, A. Masiero and L. Silvestrini, *A Complete analysis of FCNC and CP constraints in general SUSY extensions of the standard model*, *Nucl. Phys. B* **477** (1996) 321 [[hep-ph/9604387](#)].
- [96] E. Bagnaschi et al., *Likelihood Analysis of the pMSSM11 in Light of LHC 13-TeV Data*, *Eur. Phys. J. C* **78** (2018) 256 [[1710.11091](#)].
- [97] T. Falk, K. A. Olive and M. Srednicki, *Heavy sneutrinos as dark matter*, *Phys. Lett. B* **339** (1994) 248 [[hep-ph/9409270](#)].
- [98] M. Chakraborti, S. Heinemeyer and I. Saha, *Improved $(g - 2)_\mu$ measurements and wino/higgsino dark matter*, *Eur. Phys. J. C* **81** (2021) 1069 [[2103.13403](#)].
- [99] K. Griest, *Cross-Sections, Relic Abundance and Detection Rates for Neutralino Dark Matter*, *Phys. Rev. D* **38** (1988) 2357.
- [100] K. Griest and D. Seckel, *Three exceptions in the calculation of relic abundances*, *Phys. Rev. D* **43** (1991) 3191.
- [101] M. J. Baker et al., *The Coannihilation Codex*, *JHEP* **12** (2015) 120 [[1510.03434](#)].
- [102] S. Baum, M. Carena, N. R. Shah and C. E. M. Wagner, *Higgs portals for thermal Dark Matter. EFT perspectives and the NMSSM*, *JHEP* **04** (2018) 069 [[1712.09873](#)].
- [103] J. Cao, L. Meng, Y. Yue, H. Zhou and P. Zhu, *Suppressing the scattering of WIMP dark matter and nucleons in supersymmetric theories*, *Phys. Rev. D* **101** (2020) 075003 [[1910.14317](#)].
- [104] A. Pierce, N. R. Shah and K. Freese, *Neutralino Dark Matter with Light Staus*, [1309.7351](#).
- [105] L. Calibbi, J. M. Lindert, T. Ota and Y. Takanishi, *LHC Tests of Light Neutralino Dark Matter without Light Sfermions*, *JHEP* **11** (2014) 106 [[1410.5730](#)].
- [106] C. Cheung, M. Papucci, D. Sanford, N. R. Shah and K. M. Zurek, *NMSSM Interpretation of the Galactic Center Excess*, *Phys. Rev. D* **90** (2014) 075011 [[1406.6372](#)].
- [107] PANDAX-4T collaboration, Y. Meng et al., *Dark Matter Search Results from the PandaX-4T Commissioning Run*, *Phys. Rev. Lett.* **127** (2021) 261802 [[2107.13438](#)].

- [108] P. Huang and C. E. M. Wagner, *Blind Spots for neutralino Dark Matter in the MSSM with an intermediate m_A* , *Phys. Rev. D* **90** (2014) 015018 [[1404.0392](#)].
- [109] A. Crivellin, M. Hoferichter, M. Procura and L. C. Tunstall, *Light stops, blind spots, and isospin violation in the MSSM*, *JHEP* **07** (2015) 129 [[1503.03478](#)].
- [110] T. Han, F. Kling, S. Su and Y. Wu, *Unblinding the dark matter blind spots*, *JHEP* **02** (2017) 057 [[1612.02387](#)].
- [111] M. Carena, J. Osborne, N. R. Shah and C. E. M. Wagner, *Supersymmetry and LHC Missing Energy Signals*, *Phys. Rev. D* **98** (2018) 115010 [[1809.11082](#)].
- [112] ATLAS collaboration, G. Aad et al., *Search for chargino–neutralino pair production in final states with three leptons and missing transverse momentum in $\sqrt{s} = 13$ TeV pp collisions with the ATLAS detector*, *Eur. Phys. J. C* **81** (2021) 1118 [[2106.01676](#)].
- [113] CMS collaboration, A. M. Sirunyan et al., *Combined search for electroweak production of charginos and neutralinos in proton-proton collisions at $\sqrt{s} = 13$ TeV*, *JHEP* **03** (2018) 160 [[1801.03957](#)].
- [114] CMS collaboration, A. M. Sirunyan et al., *Search for electroweak production of charginos and neutralinos in multilepton final states in proton-proton collisions at $\sqrt{s} = 13$ TeV*, *JHEP* **03** (2018) 166 [[1709.05406](#)].
- [115] ATLAS collaboration, M. Aaboud et al., *Search for electroweak production of supersymmetric particles in final states with two or three leptons at $\sqrt{s} = 13$ TeV with the ATLAS detector*, *Eur. Phys. J. C* **78** (2018) 995 [[1803.02762](#)].
- [116] ATLAS collaboration, M. Aaboud et al., *Search for chargino-neutralino production using recursive jigsaw reconstruction in final states with two or three charged leptons in proton-proton collisions at $\sqrt{s} = 13$ TeV with the ATLAS detector*, *Phys. Rev. D* **98** (2018) 092012 [[1806.02293](#)].
- [117] ATLAS collaboration, G. Aad et al., *Search for direct production of electroweakinos in final states with one lepton, missing transverse momentum and a Higgs boson decaying into two b-jets in pp collisions at $\sqrt{s} = 13$ TeV with the ATLAS detector*, *Eur. Phys. J. C* **80** (2020) 691 [[1909.09226](#)].
- [118] ATLAS collaboration, M. Aaboud et al., *Search for chargino and neutralino production in final states with a Higgs boson and missing transverse momentum at $\sqrt{s} = 13$ TeV with the ATLAS detector*, *Phys. Rev. D* **100** (2019) 012006 [[1812.09432](#)].
- [119] CMS collaboration, A. M. Sirunyan et al., *Search for new phenomena in final states with two opposite-charge, same-flavor leptons, jets, and missing transverse momentum in pp collisions at $\sqrt{s} = 13$ TeV*, *JHEP* **03** (2018) 076 [[1709.08908](#)].
- [120] CMS collaboration, A. M. Sirunyan et al., *Search for supersymmetry with Higgs boson to diphoton decays using the razor variables at $\sqrt{s} = 13$ TeV*, *Phys. Lett. B* **779** (2018) 166 [[1709.00384](#)].

- [121] CMS collaboration, A. M. Sirunyan et al., *Searches for pair production of charginos and top squarks in final states with two oppositely charged leptons in proton-proton collisions at $\sqrt{s} = 13$ TeV*, *JHEP* **11** (2018) 079 [[1807.07799](#)].
- [122] ATLAS collaboration, M. Aaboud et al., *Search for photonic signatures of gauge-mediated supersymmetry in 13 TeV pp collisions with the ATLAS detector*, *Phys. Rev. D* **97** (2018) 092006 [[1802.03158](#)].
- [123] ATLAS collaboration, G. Aad et al., *Search for supersymmetry in events with four or more charged leptons in 139 fb⁻¹ of $\sqrt{s} = 13$ TeV pp collisions with the ATLAS detector*, *JHEP* **07** (2021) 167 [[2103.11684](#)].
- [124] ATLAS collaboration, G. Aad et al., *Searches for electroweak production of supersymmetric particles with compressed mass spectra in $\sqrt{s} = 13$ TeV pp collisions with the ATLAS detector*, *Phys. Rev. D* **101** (2020) 052005 [[1911.12606](#)].
- [125] ATLAS collaboration, M. Aaboud et al., *Search for electroweak production of supersymmetric states in scenarios with compressed mass spectra at $\sqrt{s} = 13$ TeV with the ATLAS detector*, *Phys. Rev. D* **97** (2018) 052010 [[1712.08119](#)].
- [126] CMS collaboration, A. M. Sirunyan et al., *Search for new physics in events with two soft oppositely charged leptons and missing transverse momentum in proton-proton collisions at $\sqrt{s} = 13$ TeV*, *Phys. Lett. B* **782** (2018) 440 [[1801.01846](#)].
- [127] CMS collaboration, A. M. Sirunyan et al., *Search for supersymmetric partners of electrons and muons in proton-proton collisions at $\sqrt{s} = 13$ TeV*, *Phys. Lett. B* **790** (2019) 140 [[1806.05264](#)].
- [128] P. Fayet, *Spontaneously Broken Supersymmetric Theories of Weak, Electromagnetic and Strong Interactions*, *Phys. Lett. B* **69** (1977) 489.
- [129] G. R. Farrar and P. Fayet, *Phenomenology of the Production, Decay, and Detection of New Hadronic States Associated with Supersymmetry*, *Phys. Lett. B* **76** (1978) 575.
- [130] F. Staub, *SARAH*, [0806.0538](#).
- [131] F. Staub, *SARAH 3.2: Dirac Gauginos, UFO output, and more*, *Comput. Phys. Commun.* **184** (2013) 1792 [[1207.0906](#)].
- [132] F. Staub, *SARAH 4 : A tool for (not only SUSY) model builders*, *Comput. Phys. Commun.* **185** (2014) 1773 [[1309.7223](#)].
- [133] F. Staub, *Exploring new models in all detail with SARAH*, *Adv. High Energy Phys.* **2015** (2015) 840780 [[1503.04200](#)].
- [134] W. Porod, *SPheno, a program for calculating supersymmetric spectra, SUSY particle decays and SUSY particle production at e+ e- colliders*, *Comput. Phys. Commun.* **153** (2003) 275 [[hep-ph/0301101](#)].
- [135] W. Porod and F. Staub, *SPheno 3.1: Extensions including flavour, CP-phases and models beyond the MSSM*, *Comput. Phys. Commun.* **183** (2012) 2458 [[1104.1573](#)].

- [136] W. Porod, F. Staub and A. Vicente, *A Flavor Kit for BSM models*, *Eur. Phys. J. C* **74** (2014) 2992 [[1405.1434](#)].
- [137] G. Belanger, F. Boudjema, A. Pukhov and A. Semenov, *MicrOMEGAs: A Program for calculating the relic density in the MSSM*, *Comput. Phys. Commun.* **149** (2002) 103 [[hep-ph/0112278](#)].
- [138] G. Belanger, F. Boudjema, C. Hugonie, A. Pukhov and A. Semenov, *Relic density of dark matter in the NMSSM*, *JCAP* **09** (2005) 001 [[hep-ph/0505142](#)].
- [139] G. Belanger, F. Boudjema, A. Pukhov and A. Semenov, *MicrOMEGAs 2.0: A Program to calculate the relic density of dark matter in a generic model*, *Comput. Phys. Commun.* **176** (2007) 367 [[hep-ph/0607059](#)].
- [140] G. Belanger, F. Boudjema, A. Pukhov and A. Semenov, *micrOMEGAs: A Tool for dark matter studies*, *Nuovo Cim. C* **033N2** (2010) 111 [[1005.4133](#)].
- [141] G. Belanger, F. Boudjema, A. Pukhov and A. Semenov, *micrOMEGAs-3: A program for calculating dark matter observables*, *Comput. Phys. Commun.* **185** (2014) 960 [[1305.0237](#)].
- [142] D. Barducci, G. Belanger, J. Bernon, F. Boudjema, J. Da Silva, S. Kraml et al., *Collider limits on new physics within micrOMEGAs*, [1606.03834](#).
- [143] P. Bechtle, O. Brein, S. Heinemeyer, G. Weiglein and K. E. Williams, *HiggsBounds: Confronting Arbitrary Higgs Sectors with Exclusion Bounds from LEP and the Tevatron*, *Comput. Phys. Commun.* **181** (2010) 138 [[0811.4169](#)].
- [144] P. Bechtle, O. Brein, S. Heinemeyer, G. Weiglein and K. E. Williams, *HiggsBounds 2.0.0: Confronting Neutral and Charged Higgs Sector Predictions with Exclusion Bounds from LEP and the Tevatron*, *Comput. Phys. Commun.* **182** (2011) 2605 [[1102.1898](#)].
- [145] P. Bechtle, O. Brein, S. Heinemeyer, O. Stål, T. Stefaniak, G. Weiglein et al., *HiggsBounds – 4: Improved Tests of Extended Higgs Sectors against Exclusion Bounds from LEP, the Tevatron and the LHC*, *Eur. Phys. J. C* **74** (2014) 2693 [[1311.0055](#)].
- [146] P. Bechtle, D. Dercks, S. Heinemeyer, T. Klingl, T. Stefaniak, G. Weiglein et al., *HiggsBounds-5: Testing Higgs Sectors in the LHC 13 TeV Era*, *Eur. Phys. J. C* **80** (2020) 1211 [[2006.06007](#)].
- [147] P. Bechtle, S. Heinemeyer, O. Stål, T. Stefaniak and G. Weiglein, *HiggsSignals: Confronting arbitrary Higgs sectors with measurements at the Tevatron and the LHC*, *Eur. Phys. J. C* **74** (2014) 2711 [[1305.1933](#)].
- [148] O. Stål and T. Stefaniak, *Constraining extended Higgs sectors with HiggsSignals*, *PoS EPS-HEP2013* (2013) 314 [[1310.4039](#)].
- [149] P. Bechtle, S. Heinemeyer, O. Stål, T. Stefaniak and G. Weiglein, *Probing the Standard Model with Higgs signal rates from the Tevatron, the LHC and a future ILC*, *JHEP* **11** (2014) 039 [[1403.1582](#)].

- [150] P. Bechtle, S. Heinemeyer, T. Klingl, T. Stefaniak, G. Weiglein and J. Wittbrodt, *HiggsSignals-2: Probing new physics with precision Higgs measurements in the LHC 13 TeV era*, *Eur. Phys. J. C* **81** (2021) 145 [[2012.09197](#)].
- [151] F. Feroz, M. P. Hobson and M. Bridges, *MultiNest: an efficient and robust Bayesian inference tool for cosmology and particle physics*, *Mon. Not. Roy. Astron. Soc.* **398** (2009) 1601 [[0809.3437](#)].
- [152] PLANCK collaboration, N. Aghanim et al., *Planck 2018 results. VI. Cosmological parameters*, *Astron. Astrophys.* **641** (2020) A6 [[1807.06209](#)].
- [153] XENON collaboration, E. Aprile et al., *Constraining the spin-dependent WIMP-nucleon cross sections with XENON1T*, *Phys. Rev. Lett.* **122** (2019) 141301 [[1902.03234](#)].
- [154] PARTICLE DATA GROUP collaboration, M. Tanabashi, K. Hagiwara, Hikasa et al., *Review of particle physics*, *Phys. Rev. D* **98** (2018) 030001.
- [155] J. E. Camargo-Molina, B. O’Leary, W. Porod and F. Staub, *Vevacious: A Tool For Finding The Global Minima Of One-Loop Effective Potentials With Many Scalars*, *Eur. Phys. J. C* **73** (2013) 2588 [[1307.1477](#)].
- [156] J. E. Camargo-Molina, B. Garbrecht, B. O’Leary, W. Porod and F. Staub, *Constraining the Natural MSSM through tunneling to color-breaking vacua at zero and non-zero temperature*, *Phys. Lett. B* **737** (2014) 156 [[1405.7376](#)].
- [157] W. Beenakker, R. Hopker and M. Spira, *PROSPINO: A Program for the production of supersymmetric particles in next-to-leading order QCD*, [hep-ph/9611232](#).
- [158] J. Alwall, M. Herquet, F. Maltoni, O. Mattelaer and T. Stelzer, *MadGraph 5 : Going Beyond*, *JHEP* **06** (2011) 128 [[1106.0522](#)].
- [159] E. Conte, B. Fuks and G. Serret, *MadAnalysis 5, A User-Friendly Framework for Collider Phenomenology*, *Comput. Phys. Commun.* **184** (2013) 222 [[1206.1599](#)].
- [160] T. Sjöstrand, S. Ask, J. R. Christiansen, R. Corke, N. Desai, P. Ilten et al., *An introduction to PYTHIA 8.2*, *Comput. Phys. Commun.* **191** (2015) 159 [[1410.3012](#)].
- [161] M. Drees, H. Dreiner, D. Schmeier, J. Tattersall and J. S. Kim, *CheckMATE: Confronting your Favourite New Physics Model with LHC Data*, *Comput. Phys. Commun.* **187** (2015) 227 [[1312.2591](#)].
- [162] D. Dercks, N. Desai, J. S. Kim, K. Rolbiecki, J. Tattersall and T. Weber, *CheckMATE 2: From the model to the limit*, *Comput. Phys. Commun.* **221** (2017) 383 [[1611.09856](#)].
- [163] J. S. Kim, D. Schmeier, J. Tattersall and K. Rolbiecki, *A framework to create customised LHC analyses within CheckMATE*, *Comput. Phys. Commun.* **196** (2015) 535 [[1503.01123](#)].
- [164] DELPHES 3 collaboration, J. de Favereau, C. Delaere, P. Demin, A. Giammanco,

- V. Lemaître, A. Mertens et al., *DELPHES 3, A modular framework for fast simulation of a generic collider experiment*, *JHEP* **02** (2014) 057 [[1307.6346](#)].
- [165] G. Alguero, J. Heisig, C. K. Khosa, S. Kraml, S. Kulkarni, A. Lessa et al., *Constraining new physics with SModelS version 2*, *JHEP* **08** (2022) 068 [[2112.00769](#)].
- [166] B. Fuks, M. Klasen, D. R. Lamprea and M. Rothering, *Gaugino production in proton-proton collisions at a center-of-mass energy of 8 TeV*, *JHEP* **10** (2012) 081 [[1207.2159](#)].
- [167] B. Fuks, M. Klasen, D. R. Lamprea and M. Rothering, *Precision predictions for electroweak superpartner production at hadron colliders with RESUMINO*, *Eur. Phys. J. C* **73** (2013) 2480 [[1304.0790](#)].
- [168] H. Baer, V. Barger, P. Huang and X. Tata, *Natural Supersymmetry: LHC, dark matter and ILC searches*, *JHEP* **05** (2012) 109 [[1203.5539](#)].
- [169] J. Cao, Y. He, L. Shang, Y. Zhang and P. Zhu, *Current status of a natural NMSSM in light of LHC 13 TeV data and XENON-1T results*, *Phys. Rev. D* **99** (2019) 075020 [[1810.09143](#)].
- [170] ATLAS collaboration, G. Aad et al., *Search for charginos and neutralinos in final states with two boosted hadronically decaying bosons and missing transverse momentum in pp collisions at $\sqrt{s} = 13$ TeV with the ATLAS detector*, *Phys. Rev. D* **104** (2021) 112010 [[2108.07586](#)].
- [171] J. Cao, D. Li, J. Lian, Y. Yue and H. Zhou, *Singlino-dominated dark matter in general NMSSM*, *JHEP* **06** (2021) 176 [[2102.05317](#)].
- [172] ILC collaboration, *The International Linear Collider Technical Design Report - Volume 2: Physics*, [1306.6352](#).
- [173] CLIC DETECTOR, PHYSICS STUDY collaboration, H. Abramowicz et al., *Physics at the CLIC $e+e-$ Linear Collider – Input to the Snowmass process 2013*, in *Community Summer Study 2013: Snowmass on the Mississippi*, 7, 2013, [1307.5288](#).
- [174] CLICDP, CLIC collaboration, T. K. Charles et al., *The Compact Linear Collider (CLIC) - 2018 Summary Report*, [1812.06018](#).
- [175] M. Chakraborti, S. Heinemeyer and I. Saha, *Improved $(g - 2)_\mu$ Measurements and Supersymmetry : Implications for e^+e^- colliders*, in *International Workshop on Future Linear Colliders*, 5, 2021, [2105.06408](#).